THESIS FOR THE DEGREE OF DOCTOR OF PHILOSOPHY
IN SOLID AND STRUCTURAL MECHANICS

Influence of railway wheel tread damage and track properties on wheelset durability – Field tests and numerical simulations

MICHELE MARIA MAGLIO

Department of Mechanics and Maritime Sciences
CHALMERS UNIVERSITY OF TECHNOLOGY
Gothenburg, Sweden, 2023

Influence of railway wheel tread damage and track properties on wheelset durability – Field tests and numerical simulations
MICHELE MARIA MAGLIO
ISBN 978-91-7905-764-0

Doktorsavhandlingar vid Chalmers tekniska högskola
Ny serie nr 5230
ISSN 0346-718X

Department of Mechanics and Maritime Sciences
Chalmers University of Technology
SE-412 96 Gothenburg
Sweden
Telephone + 46 (0)31-772 1000

Cover: A railway wheel with severe tread damage.

Chalmers Reproservice

Gothenburg, Sweden 2023

Influence of railway wheel tread damage and track properties on wheelset durability – Field tests and numerical simulations

MICHELE MARIA MAGLIO
Department of Mechanics and Maritime Sciences
Chalmers University of Technology

ABSTRACT

Wheel tread damage leading to high magnitudes of vertical wheel–rail contact forces is a major cause of train delays in the Swedish railway network, particularly during the coldest months of the year. According to regulations, vehicles generating wheel–rail impact loads exceeding the limit values must be taken out of service for wheel maintenance. This may lead to severe traffic disruptions and associated high costs. On the other hand, increased wheel–rail impact loads cause elevated stress levels in wheels, axles and bearings and may shorten the life of track components, resulting in higher costs for vehicle and track maintenance. Thus, alarm limits should provide a balance between preventing operational failures and minimising the number of stopped trains.

The aim of this thesis is to enhance the understanding of the consequences of wheel tread damage and to identify better means of addressing them. To achieve this aim, the ability of numerical simulations to investigate different operational scenarios is crucial. A versatile and cost-efficient method to simulate the vertical dynamic interaction between a wheelset and a railway track, accounting for generic distributions and shapes of wheel tread damage, has therefore been extended and improved. The dynamic coupling between the two contact points (one on each wheel) via the wheelset axle and via the rails and sleepers is accounted for. Post-processing steps to evaluate fatigue impact at critical positions in the wheelset have been developed.

The applied simulation models have been calibrated and verified by extensive field tests. Measurement campaigns with two different Swedish passenger trains have been carried out. In the first field test, impact loads generated by a wheelset with severe tread damage were measured. Measurements and simulations have been used to illustrate how wheel–rail loads and fatigue impact depend on the three-dimensional shape of the tread damage. The effects of speed and travelling direction of the vehicle, position in the sleeper bay where the defect strikes the rail, lateral position of the wheelset, and track stiffness on wheel–rail contact forces and wheelset durability have been investigated.

In the second long-term field test, axle stresses have been monitored using an instrumented wheelset on a passenger train in revenue traffic. By post-processing of test results, statistical models of stress spectra for different stretches of the Swedish rail network were obtained. Moreover, the parameters describing such models have been related to track characteristics in terms of the presence of curves, switches & crossings and irregularities in track geometry. This allowed to develop numerical routines to evaluate wheelset durability depending on operational parameters. These studies are used to initiate a discussion on improved wheelset maintenance procedures.

Keywords: railway wheel tread damage, dynamic wheel–rail interaction, wheel–rail impact loads, instrumented wheelset, axle stresses, wheelset durability, rail vehicle maintenance.

SAMMANFATTNING

Löpbaneskador på hjul som leder till höga vertikala kontaktkrafter mellan hjul och räl är en av de främsta orsakerna till tågförseningar i det svenska järnvägsnätet, särskilt under årets kallaste månader. Om ett fordon genererar dynamiska kontaktkrafter som överstiger det tillåtna gränsvärdet ska fordonet tas ur drift för hjulunderhåll. Detta kan leda till allvarliga trafikstörningar och höga kostnader för operatörer. Ökade belastningar orsakar även förhöjda spänningsnivåer i hjul, axlar och lager och kan förkorta livslängden hos spårkomponenter. Detta resulterar i högre kostnader för fordons- och spårunderhåll. Därför bör gränsvärdet väljas så att riskerna för driftfel och antalet stoppade tåg balanseras.

Syftet med denna avhandling är att öka förståelsen för konsekvenser av skador på hjulets löpbana och att identifiera bättre sätt att hantera dem. Numeriska simuleringar har använts för att bedöma risker kopplade till olika scenarier. En kostnadseffektiv metod för att simulera den vertikala dynamiska interaktionen mellan ett hjulpar och ett järnvägsspår har därför utökats och förbättrats. Metoden tar hänsyn till generiska fördelningar och former av skador på hjulets löpbana, samt till den dynamiska kopplingen mellan de två kontaktpunkterna (en på varje hjul) via hjulparets axel och via rälerna och sliprarna. Procedurer för att beräkna påkänningar i de positioner hos hjulparet som är mest utsatta för utmattning har utvecklats.

Den tillämpade simuleringsmodellen har kalibrerats och verifierats via omfattande fältförsök med två olika svenska persontåg. I det första testet användes en hjulskadedetektor för att mäta dynamiska kontaktkrafter som genererades av ett hjulpar med allvarliga löpbaneskador. Mätningarna och motsvarande simuleringar har utvärderats för att undersöka hur stötbelastningen mellan hjul och räl och den resulterande utmattningspåkänningen beror på skadans tredimensionella form. Inverkan av fordonets hastighet och färdriktning, position i ett sliperspann där defekten träffar rälen, hjulparets laterala position samt spårstyvhet på kontaktkrafter mellan hjul och räl och hjulparets livslängd har studerats.

I det andra fältförsöket har axelspänningar övervakats med hjälp av ett instrumenterat hjulpar. Statistiska modeller av spänningsspektra för olika sträckor av det svenska järnvägsnätet har genererats. Dessutom har parametrarna som beskriver sådana modeller relaterats till förekomsten av kurvor, antalet växlar och korsningar, och avvikelser i spårgeometrin. Detta bidrar till utvecklingen av numeriska rutiner för utvärdering och förbättring av hjulparets underhållsbehov beroende på driftsparametrar.

Nyckelord: löpbaneskada, dynamisk interaktion mellan hjul och räl, stötlast, instrumenterat hjulpar, axelspänningar, livslängd, underhåll av järnvägsfordon.

Claude Monet, *Le train dans la niege*, Public domain, via Wikimedia Commons https://www.marmottan.fr/notice/4017/

PREFACE

The work presented in this thesis was accomplished at the Division of Dynamics at the Department of Mechanics and Maritime Sciences, Chalmers University of Technology, between February 2018 and December 2022. It was conducted as part of the activities within the National Centre of Excellence in Railway Mechanics CHARMEC (CHAlmers Railway MEChanics, www.charmec.chalmers.se) within the project TS20 – "Wheel tread damage – identification and effects". Parts of the research have been funded within the European Union's Horizon 2020 research and innovation programme in the Shift2Rail projects In2Track2 under grant agreement No. 826255 and In2Track3 under grant agreement No. 101012456. The project has been supported by CHARMEC's industrial partners. In particular, the support from Alstom/Bombardier Transportation, Faiveley Transport, Green Cargo, Lucchini RS, Lucchini Sweden, SJ and Trafikverket is gratefully acknowledged. The author would like to thank the members of the MU and TS20 projects Reference Group for their valuable input: Mr Roger Deuce (Alstom), Mr Pär Söderström (SJ), Mr Erik Kihlberg (Lucchini Sweden), Dr Matthias Asplund, Dr Martin Schilke and Ms Malin Syk (Trafikverket), Dr Stephan Scheriau (voestalpine) and Prof Sebastian Stichel (KTH).

ACKNOWLEDGEMENTS

First of all, I would like to thank my supervisors: thank you to my main supervisor, Professor Elena Kabo, for the great care that you have shown to me since when I was a Master Thesis student at CHARMEC, for introducing me to the world of academia and for always striving to achieve what was best for me on my journey towards the PhD defence as well as for my career. Thank you to my examiner Professor Anders Ekberg for always being available for discussion, for sharing research ideas, for guiding me in this project with such enthusiasm and for being a role model in research and academic teaching. Thank you for always showing trust and appreciation for my work. Thank you, Professor Jens Nielsen, for having guided me in the world of railway dynamics in these years. I have really appreciated your patience, your assistance, your pedagogical approach and the care for my growth as a researcher. Thank you Associate Professor Tore Vernersson for always having been available to help me, for always finding time to give feedback and for coming up with new ideas. Your help and company made field measurements much more productive and fun.

Thank you to all the members of the project reference group, to my co-authors and to all the people in CHARMEC for the fruitful discussions we have had during these years and for all the interesting research seminars and social events we have participated in. A special thank you to all my cheerful colleagues and friends at the divisions of Dynamics and Material and Computational Mechanics, as well as to Luigi, Anna-Lena, Carina and Pernilla. You made the third floor of the M-building such a pleasant work environment. Meeting my friends at work every day has made such a huge difference: our fikas, lunches, afterworks, and evenings out in Gothenburg made these years at Chalmers great! I am looking forward to keeping in touch with you and to arranging more activities with you.

I am thankful to Lucchini for the great collaboration in field tests and especially to Erik Kihlberg, Andrea Ghidini and Steven Cervello for arranging my research visit in Lovere. Thank you to all the employees of the Metallurgy, R&D and EMIT groups and to Lorenzo Ghidini for taking great care of me and for guiding me with enthusiasm throughout the development and production processes of wheels and axles.

I would like to thank every single student who actively participated during tutorials and consultations, or with whom I simply had a chat or discussion during lecture breaks, in my office or around campus. You made teaching one of the very best parts of my time as a PhD student. Thanks for your patience if I sometimes used our classes to practice Swedish (or French). I hope that you could learn from me as much as I could learn from you.

Finally, I want to express my gratitude to my parents Maria Rosaria and Massimo, as well as to my sister Martina. Although we have been living in different regions for years, you still succeed in making me feel your love and support and in always being there for me. Thank you to my uncle Zio Do. A big thank you to all my friends in my hometown Maglie and to those from my years in Torino, I am always looking forward to spending time with you during our vacations or whenever we have the chance to meet. I am grateful for being in contact with you and for having had you all by my side during these years.

Gothenburg, December 2022

Michele Maglio

THESIS

This thesis consists of an extended summary and the following appended papers:

Paper A	M. Maglio, A. Pieringer, J.C.O. Nielsen, T. Vernersson. Wheel–rail impact loads and axle bending stress simulated for generic distributions and shapes of discrete wheel tread damage, *Journal of Sound and Vibration*, vol 502, article 116085, 19 pp, 2021
Paper B	M. Maglio, T. Vernersson, J.C.O. Nielsen, A. Pieringer, P. Söderström, D. Regazzi, S. Cervello. Railway wheel tread damage and axle bending stress – Instrumented wheelset measurements and numerical simulations, *International Journal of Rail Transportation*, vol 10(3), pp 275-297, 2021
Paper C	M. Maglio, E. Kabo, A. Ekberg. Railway wheelset fatigue life estimation based on field tests, *Fatigue & Fracture of Engineering Materials and Structures*, vol 45(9), pp 2443-2456, 2022
Paper D	M. Maglio, E. Kabo, A. Ekberg. Relating the influence of track properties to axle load spectra through onboard measurements. *Submitted for international publication*
Paper E	M. Maglio, T. Vernersson, J.C.O. Nielsen, A. Ekberg, E. Kabo. Influence of railway wheel tread damage on wheel–rail impact loads and the durability of wheelsets. *To be submitted for international publication*

Contributions to co-authored papers

The appended papers were prepared in collaboration with the co-authors. The author of this thesis was responsible for the major progress of the work and for the following tasks:

- **Paper A**: Taking part in planning the paper, developing the theory and the numerical implementations, running the simulations, writing the paper, managing the submission and peer-review process.

- **Paper B:** Taking part in planning the paper and the field tests, developing the theory and the numerical implementations, planning and performing measurement activities, running the simulations, writing the paper, managing the submission and peer-review process.

- **Paper C:** Taking part in planning the paper and the field tests, developing the theory and the numerical implementations, post-processing results from the field test, running

the simulations and writing the paper, managing the submission and peer-review process.

- **Paper D:** Taking part in planning the paper and the field tests, developing the theory and the numerical implementations, running the simulations and writing the paper, managing the submission process.

- **Paper E:** Taking part in planning the paper, developing the theory and the numerical implementations, planning and performing 3D scanning of damaged wheels, post-processing results from the field test, running the simulations and writing the paper.

Other publications related to this thesis:

1. M. Maglio, M. Asplund, J.C.O. Nielsen, T. Vernersson, E. Kabo, A. Ekberg. Digitalisation of condition monitoring data as input for fatigue evaluation of wheelsets, *Proceedings of the XIX International Wheelset Congress (IWC2019),* Venice, Italy, 5 pp, 2019

2. M. Maglio, E. Kabo, A. Ekberg, P. Söderström, D. Regazzi, S. Cervello. Prediction of axle fatigue life based on field measurements, *Proceedings of the World Congress on Railway Research 2022* (WCRR2022), Birmingham, United Kingdom, 6 pp, 2022

Additional publications by the author:

1. E. Kabo, A. Ekberg, M. Maglio. Rolling contact fatigue assessment of repair rail welds, *Proceedings of the 11th International Conference on Contact Mechanics and Wear of Rail/Wheel Systems (CM2018),* Delft, The Netherlands, September 2018, pp 450-456

2. E. Kabo, A. Ekberg, M. Maglio. Rolling contact fatigue assessment of repair rail welds, *Wear*, vol 436-437, 8 pp, 2019

3. P. Torstensson, E. Aggestam, M. Maglio, J.C.O. Nielsen, T. Jerson, M. Ögren, A. Genell. Rail acceleration induced by train pass-by – Field measurements and validation of a simulation model, In: A. Orlova, D. Cole (editors): *Advances in Dynamics of Vehicles on Roads and Tracks II (Proceedings of the 27th Symposium of the International Association of Vehicle System Dynamics, IAVSD 2021, August 17–19, 2021, Saint Petersburg, Russia),* Springer, pp 302-311, 2022

4. J. Brouzoulis, L. Josefson, K. Fass, T. Andersson, M. Maglio, S. Jackman, A. Janssens. Orbital friction welding of steel bars - Heat generation and process modelling. *Submitted for international publication*, 14 pp, 2022

CONTENTS

Part I

Extended Summary

1 Introduction

1.1 Background and motivation

In order to achieve a fair and more sustainable future for the world population, the United Nations (UN) have developed a call for action in the form of 17 Sustainable Development Goals (SDG), see Figure 1 [1]. These interconnected goals aim for promoting prosperity while protecting the planet. All nations, independently of their wealth and size, are supposed to collaborate in order to accomplish these goals by 2030.

The work presented in this thesis relates to several of the SDGs. For example, goal number 9 that involves the "building of resilient infrastructure, promoting of sustainable industrialisation and fostering of innovation", and goal number 13 "Climate action".

Railways is an environmentally friendly means of transportation. Thereby, investing in railways aids in achieving both SDGs 9 and 13. Essential reasons why railways are environmentally efficient are the high stiffness and the low friction in the wheel–rail contact, which leads to low rolling resistance and energy consumption [2]. However, the wheel–rail contact is also subjected to very high stress levels that can cause material deterioration which leads to needs for maintenance.

Figure 1: The seventeen sustainable development goals [1]

In order to facilitate a shift of travellers to railways from other means of transport, trains have to be perceived as punctual and reliable. Since 2012, the punctuality rate (i.e. the share of trains that arrive at their final destination with a delay of at most 5 minutes) for passenger trains in Sweden is steady at around 90% (it was 88.2% in the third quarter of 2022 [3]). The aim agreed upon by the industry is to raise this rate to 95% [4]. To achieve this goal, improvements are required on both the infrastructure and vehicle sides. In particular, maintenance planning is of vital importance to increase the fleet availability and avoid operational disruptions.

Maintenance carries additional costs for both the train operator and the track owner. It is estimated that the degradation of the vehicle–track system corresponds to up to 60% of the total maintenance costs for the track, and almost all of the maintenance costs for the running gear [5]. With the increasing demands on railway transportation of both goods and passengers, more trains are expected to run on the same infrastructure, and possibly at higher speeds and with higher axle loads. At the same time the number and lengths of available maintenance slots have decreased. Unless actions are taken, this will increase the overall state of deterioration of vehicles. The increased loads and number of vehicles lead to higher probabilities of wheelset and rail failures. These failures usually do not pose major safety issues but can cause significant traffic disruptions which are costly for the industry and cause annoyance to passengers. In addition, derailments can in some cases have very severe consequences. One example is the derailment of a wagon carrying liquefied petroleum gas in Viareggio (Italy) in 2009, which caused 32 deaths [6]. This derailment was claimed to be caused by an axle rupture [7], which is the most common cause of derailments in Europe [8].

A better knowledge of root causes and the mechanisms that cause the deterioration of axles, wheels and rails is needed in order to reduce damage and thereby alleviate the risks of traffic disruptions, increased maintenance costs and safety issues. This knowledge could be based on condition monitoring using data from sensors installed in the tracks or on the trains. In combination with numerical predictions, such data can be used to better understand the current status of the railway assets and adapt future operations, as well as improve the design of new components, to benefit the needs of the industry. However, as discussed later in this thesis, more research is needed on methods that interpret on-board measurements to obtain useful information on asset health status, as well as in the design of algorithms to integrate measured data into predictive maintenance of assets [9].

Another challenge for the railway industry is related to noise emissions. Although environmental noise from railways can sometimes be perceived as less disturbing than that from road or air traffic [10], trains often travel on tracks that are close to dwellings and can cause severe annoyance to residents. Railway noise is generated by different sources [11]. The power unit is the main source of noise at standstill and at speeds lower than about 60 km/h, while at speeds higher than 300 km/h, aerodynamic effects are predominant. In the range of speeds in between, the main source of noise emission is the dynamic interaction between wheels and rails [11]. In particular, rolling noise is caused by roughness of the running surfaces of wheel and rail, while impact noise is generated by discrete irregularities, such as wheel flats. Both surface roughness and discrete irregularities are symptoms of material deterioration.

In summary, the work on wheel tread damage and track properties presented in this thesis relates to component deterioration. The core aim of the work – to better prevent, understand the consequences of, and maintain wheel damage – serves to improve safety, environment, economy, reliability and punctuality. This relates to a competitive advantage of the railway, as well as a means to fulfil the UN sustainable development goals.

1.2 Overview

Defects on the running surfaces of train wheels lead to dynamic wheel–rail contact forces with magnitudes that depend on train speed, axle load, the geometric shape of the irregularity and the dynamic characteristics of the vehicle–track system. For the wheelset, high vertical loads may imply an increased risk of wheel and axle fatigue, and damage of bearings. To limit the risk of a catastrophic failure of the running gear (and track), there are operational limits on allowed wheel impact loads.

Based on results from field measurements and a simulation model of dynamic vehicle–track interaction, the research presented in this thesis allows for a prediction of the vertical wheel–rail contact forces that are generated by different types of wheel tread damage as well as by irregularities in the track geometry or variations in the track properties. These results are used to predict wheelset stresses occurring during service and can be related to an increased risk of early failure. As the use of condition monitoring via instrumented assets is becoming more common in the railway industry [12], a correct interpretation of measurement data collected during service can be used to obtain real-time information on the loading and the health status of components. A deeper knowledge of the loading and the durability of railway vehicle components can be used to adopt condition-based or predictive maintenance approaches, which can lead to increased operational safety, higher utilisation rate of the fleet and savings for the track owner and the railway operator.

More in detail, in **Paper A**, a numerical procedure for the simulation of dynamic vehicle–track interaction is developed and presented. Simulations are employed to predict wheel–rail contact forces and axle stresses due to different distributions of damage on the wheel tread (the running surface of the wheel). Analytical formulations are used to model some possible geometries of discrete tread damage. The dynamic coupling between the two contact points (one on each wheel) via the wheelset axle and via the rail and sleepers is accounted for. Using this procedure implemented in an in-house software, the influence of tread damage and operational conditions on wheel–rail contact forces and axle stresses is analysed in an extensive parametric study.

In **Paper B**, the measured evolution of wheel tread damage over time is used as input in an in-house software to compute stresses in a wheelset. In parallel, a physical wheelset in traffic has been instrumented with strain gauges on its axle. The measured and calculated spectra of dynamic stresses under operational conditions are compared. The relative effects of the measured wheel out-of-roundness (OOR) and specified levels of rail roughness on axle bending stresses are investigated.

In **Paper C**, axle stress spectra collected during an extensive field test campaign over different stretches of the Swedish railway network are modelled using statistical distributions. Time histories of axle bending stress are generated from the statistical distributions using a Monte Carlo approach. These simulated histories are then used in fatigue life analyses by applying different fatigue assessment algorithms and different assumptions on the maintenance status of the axle. Fatigue lives obtained using measured or simulated stress histories show a good match. The method can also be used to assess the effects of overloads, small surface cracks in the axle, and variations in track properties on axle durability.

In **Paper D**, the measured axle stress spectra and the occurrence of overloads on some stretches of the Swedish railway network are related to the numbers of switches, bridges and tunnels, the distributions and radii of circular and transition curves, and other parameters used to describe the track geometry and stiffness. The dependence between these parameters and the statistical distributions used to model the stress spectra, as well as the occurrence of stress overloads for the respective stretches, are shown. This allows to predict the effect that different track characteristics could have on wheelset durability. Results in terms of measured axle stresses are verified by performing quasistatic FE analyses based on wheel–rail contact forces computed from multibody simulations.

Paper E is focused on wheel–rail impact loads and wheelset damage generated by some different types of severe tread damage. In a full-scale field test, a damaged wheelset on a passenger coach travelled through a wayside wheel impact load detector (WILD) at different train speeds. The entire tread, including the tread damage, was scanned by means of a 3D laser equipment. The geometry of the wheel tread is employed in simulations of dynamic vehicle–track interaction. For different operational parameters, the simulated results are compared with field measurements. The influence of the increased load levels on the fatigue of the wheel rim, the wheel hub and the bearings, as well as on the initiation of subsurface fatigue in wheels, is assessed.

Overall, these studies on fatigue damage caused by different combinations of wheel tread defects and operational conditions can help in developing and adopting a condition-based or predictive maintenance approach for critical components in the running gear.

1.3 Outline of the thesis

The extended summary of this thesis is structured as follows:

In Chapter 2, some fundamental aspects of dynamic train–track interaction, and of wheelset and track design, are presented. Different forms of wheel tread damage and rail surface deterioration are described. Some aspects of maintenance planning are discussed.

Chapter 3 deals with vertical dynamic wheel–rail contact forces and how the magnitudes of these are affected by discrete damage on the running surfaces of wheels and rails. Methods to measure or numerically predict such loads are described.

Chapter 4 introduces stresses in the axle, wheels and bearings and some techniques that are used to monitor these. Procedures to numerically predict stress levels in the wheelset are also discussed.

Chapter 5 discusses the on-going shift towards optimised maintenance procedures in the railway industry and how the presented work fits in this context.

A summary of the appended papers is presented in Chapter 6.

Finally, Chapter 7 concludes the work and presents some ideas for future research.

2 Wheel tread and rail surface damage

2.1 Wheelset and track components

The wheel–rail contact is the interface between the running gear and the track. The running gear consists of the wheelsets (axle and wheels), the bogie, the primary and secondary suspensions and the bearing boxes. Some simpler vehicles, named rigid-frame vehicles, do not have a bogie nor a secondary suspension [13]. The running gear supports the carbody, guides the vehicle, is used for braking and can provide traction to the vehicle [14]. The wheelset includes two wheels, which in almost all cases are rigidly connected by an axle. As a consequence, the whole wheelset spins around its axial axis with a uniform angular velocity. The wheelset steers based on the conicity of the wheel running surfaces, which are denoted wheel treads. If the centre of the wheelset is displaced in the lateral direction, the two wheels make contact with the rails at points with different rolling radii. The difference in rolling velocity between the two contact points allows the vehicle to steer. Figure 2 illustrates the terminology used to refer to some parts of the wheelset and the track.

The components of the track are separated into superstructure and substructure. The rails, sleepers and ballast (or slabs), as well as their elastic connections, are part of the superstructure. The rails are mounted to the sleepers via fastenings and rail pads. The rails have an inclination

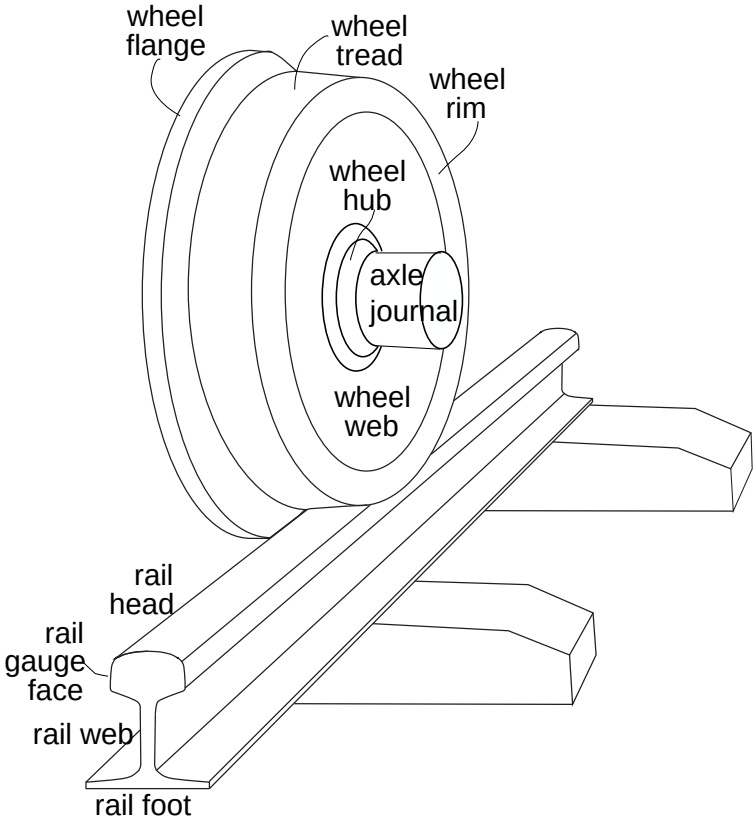

Figure 2: Terminology used to refer to some parts of the wheelset and of the track

which allows for a better fit with the wheel profile. The profile match between the wheel tread and the rail running surface determines the guiding performance of the train. The substructure usually consists of the subgrade, which in some cases is replaced by bridge or tunnel structures [15] which may lead to variations in track stiffness.

2.2 Damage on wheel treads

A comprehensive guide on different forms of wheel tread damage has been presented by Deuce [16]. High wheel–rail contact forces may lead to plastic deformation, in particular when the contact is close to the field side of the wheel or the gauge corner of the rail. The wheel tread is affected by wear, which is a gradual removal of material due to adhesion and sliding in the wheel–rail contact [17]. In some cases, the tread wear is fairly benign, see Section 2.4, but wheels mainly rolling on straight routes and/or equipped with tread brakes may develop hollow tread wear. The wear is in this case concentrated to the centre of the tread, see Figure 3. This leads to changes in the conicity of the wheel tread and possibly to the formation of a "false flange" towards the field side of the wheel [16].

Regular contact between the wheel flange and the rail gauge corner due to poor steering or (lateral) track geometry irregularities may lead to severe wear of the wheel flange. If this happens, the contact position on the opposite wheel during curving may shift to a position closer to its field side. As a result, the steering performance of the train is impaired.

Wear of the wheel tread can also generate out-of-roundness (OOR), which can be a periodic (polygonisation) or stochastic variation in radius around the circumference [18]. The latter case can be a consequence of the presence of a mixed microstructure on the wheel tread generated by inadequate heat treatment during production [16].

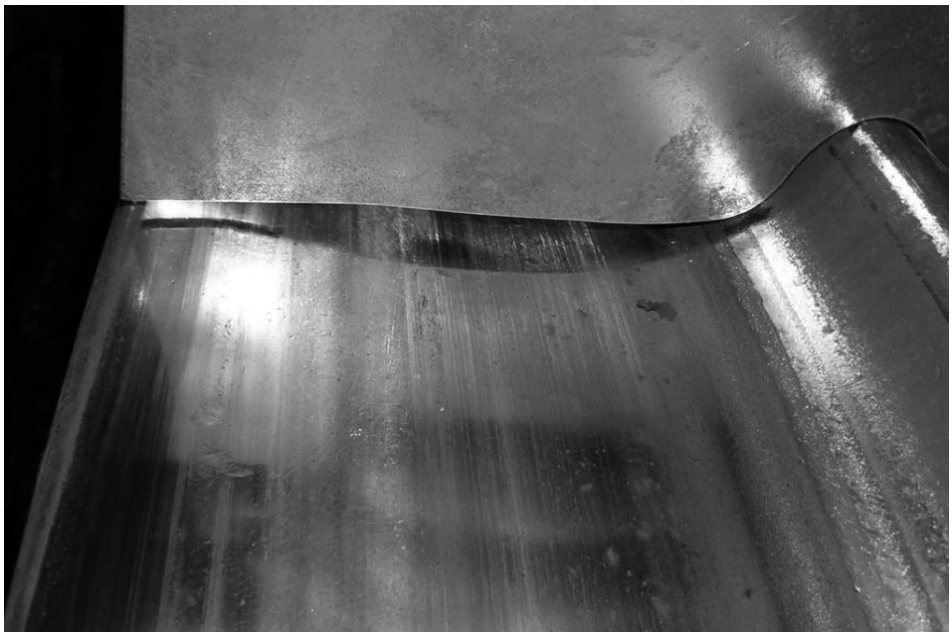

Figure 3: Hollow wear on a locomotive wheel. Picture courtesy of A. Ekberg

The tangential creep forces that are generated in the wheel–rail contact contribute to the initiation of cracks on the wheel tread. Rolling contact fatigue (RCF) defects may form on the wheel tread as cracks that start at a shallow inclination from the surface before they typically deviate to a more radial growth direction. If the cracks interact and there is material fall-out, so-called RCF clusters may form quickly. In some cases, RCF clusters can be distributed over the entire wheel tread in the circumferential direction, see Figure 4. In other cases, RCF clusters

Figure 4: Wheel with severe RCF damage

Figure 5: Wheel with isolated RCF defects

only cover patches of the wheel tread, or single isolated RCF defects (which can still reach significant depths) can be observed, see Figure 5. In this thesis, wheels with RCF damage have been studied in **Paper B** and **Paper E**.

Crack growth in RCF affected areas of the tread can be enhanced by the penetration of liquids or snow in between the crack faces. RCF clusters are particularly common during the winter season. Indentations are another type of discrete defects, see Figure 6. These are usually caused by gravel/sand or other loose particles on the rail. Their effect is often mainly cosmetic [16] as they do not generate significant variations in wheel–rail contact forces [19], see also the field test described in **Paper E**.

Elevated temperatures due to tread braking can along with tractional wheel–rail contact forces generate thermal cracks [20]. Such cracks can also grow and generate RCF clusters in the wheel rim [21].

Locked wheels sliding on the rail may lead to severe wear and overheating of the wheel material followed by a rapid cooling (when the wheel starts to roll again) of a section of the wheel tread. This results in a characteristic form of wheel tread damage denoted wheel flat. The reason for the sliding may be that the brakes are poorly adjusted, frozen or defective, or that the braking force is too high in relation to the available wheel/rail adhesion [22]. Newly formed wheel flats tend to have sharp edges, which round off over time due to the repeated impacts on the rail [23]. Some examples of wheel flats are shown in Figures 7 and 8. If the steel in the heat affected zone on the wheel is subjected to martensite formation, it becomes harder and more brittle.

Figure 6: Wheel with indentations on the tread. The black and white dots were used as markings during the 3D scanning activities of **Paper E**

Figure 7: Wheel with a large wheel flat

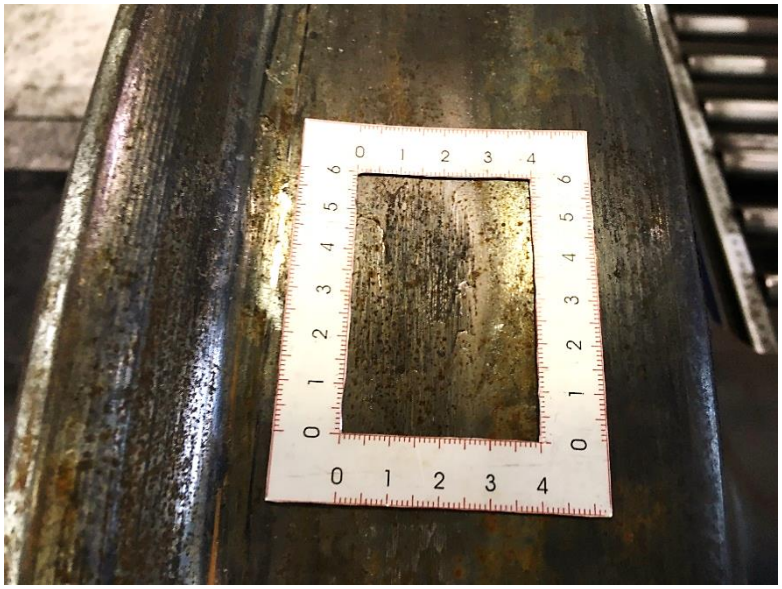

Figure 8: Wheel with a small wheel flat

Subsequent mechanical loads on the wheel may cause crack formation and further material fall-out or spalling of the martensitic steel.

Another possible cause of deviations in wheel tread geometry is the addition of material due to block braking. During prolonged braking, cast iron blocks may overheat and block material can partially melt and stick to the wheel surface in a process that reminds of welding. Sometimes

Figure 9: Material addition from brake blocks during tread braking

this process can occur where other tread defects were present, see Figure 9. Unlike the more frequently occurring forms of wheel tread damage, these defects are not due to the loss of wheel material. However, they still generate sharp variations in the wheel–rail contact geometry and, subsequently, high impact loads.

2.3 Monitoring of wheel tread damage

The studies in this thesis are mainly aimed at assessing the influence of the deterioration of the wheel tread on dynamic wheel–rail contact forces and resulting stresses and damage in the wheelset. The presence of wheel tread damage can be detected by means of condition monitoring and visual inspections. For example, wheel flats and severe RCF damage can be detected using data from wayside wheel impact load detectors (WILDs) ([19],[24], **Paper E**), from acoustic sensors mounted on the train or in the track, or by visual inspections.

Tread wear can be quantified by means of measurements such as those performed in **Paper B** and **Paper E**. In these papers, three different types of measurements have been performed: wheel profile measurements (at selected positions around the circumference), OOR measurements (radial deviation from the nominal wheel radius on different rolling circles) and 3D scans of the wheel tread.

The lateral wheel profile is usually measured in order to detect tread wear (for example hollow wear), and, among other possible applications, it can be used to predict the wheel–rail contact position for some given conditions, see **Paper B**. In this research project, MiniProf [25] has been used to measure the wheel lateral profiles, see Figure 10.

Figure 10: Measurement of the wheel profile used in the simulations of **Paper B**

In **Paper B**, wheel OOR measurements have been used to assess the effect of tread deterioration on dynamic vertical wheel–rail contact forces and axle stresses. OOR was measured using either an in-house measurement device or the commercial equipment named TriTops [26], see Figure 11. The two devices are based on the same principle, where the wheelset is lifted from the rail and the wheel is rotated manually. Displacement probes measure the radial profile of the wheel tread around selected rolling circles. At the same time, a pulse wheel keeps track of the circumferential location where the OOR is being measured.

Figure 11: Measurement of wheel OOR for **Paper B**. *The pulse wheel (upper part of the figure) and the measurement probes (centre part of the figure) of the commercial equipment TriTops can be observed [26]*

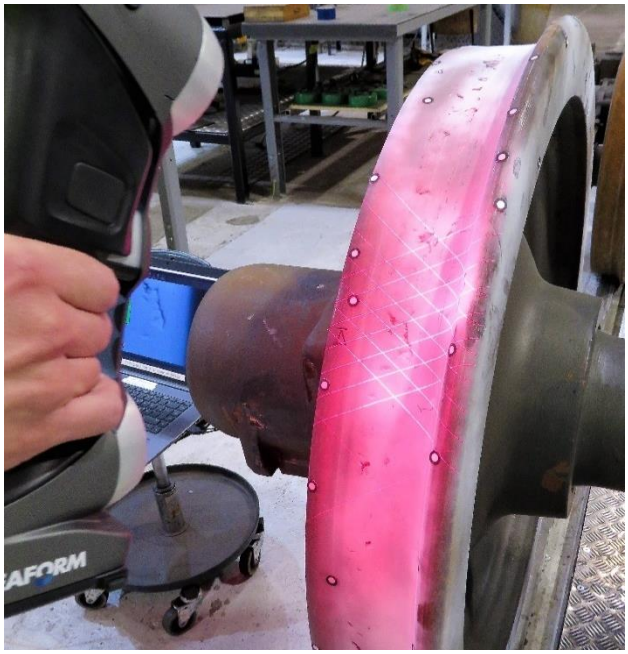

Figure 12: 3D scanning of a damaged tread surface. The generated virtual 3D surface is visible on the laptop in the background

In the field tests of **Paper B** and **Paper E**, the wheel treads were scanned by means of the commercial optical laser equipment named HandyScan [27]. The portable 3D scanner is connected to a computer where a commercial software named VXinspect [28] is installed. The software generates a virtual 3D surface in real time while the scanning activity is carried out. The scanner has a maximum measurement accuracy of 0.03 mm, which allows for a very detailed characterisation of tread defects. The scans can then be post-processed and used in simulations of dynamic wheel–rail interaction, see **Paper E**. An example of a 3D scanning activity is shown in Figure 12. The wheel surface is sprayed with talcum-based powder in order to avoid reflections from the wheelset steel. Some black and white dots are distributed on the wheel tread to be used as reference points by the software.

Data from instrumented wheelsets are extensively used in **Papers B – D** of this thesis. The interpretation of measurement data can be valuable for detecting damage growth on the wheel tread. Wheelsets can be instrumented with strain gauges that can be used to monitor wheel–rail contact forces [29] or axle stresses [30]. A relatively cheap but simple solution is the use of accelerometers on axle-boxes [31]. One of the advantages of using instrumented assets is the possibility to simultaneously monitor the health status of the vehicle and of the track. However, more knowledge is needed on how to distinguish the effects of wheelset and track characteristics on the measurement results. This topic is dealt with in **Paper D**.

Whether a train affected by wheel tread damage can continue running or not is mainly determined by regulations regarding the maximum allowed size of wheel and rail damage. These regulations differ between different countries. In general, the infrastructure managers decide which limits are applied [32]. The main infrastructure manager in Sweden is Trafikverket (the Swedish Transport Administration).

For a long time, regulations in the Nordic countries have been based on the longitudinal size and depth (or height) of damage. On the tracks owned by Trafikverket, if a wheel flat or another type of tread defect was suspected to be longer than 60 mm or if it consisted of a build-up of material on the tread with a suspected height of more than 1 mm, the vehicle had to be run at a maximum speed of 10 km/h. For wheel flats with lengths in between 40 and 60 mm, the vehicle could proceed to its final destination but without embarking new cargo [33]. Inlandsbanan AB, a minor Swedish track owner, applies further restrictions for damage with length between 40 and 60 mm if the temperature is below -10 °C [34]. In Norway, the allowable length of tread damage depends on the wheel diameter [35]. It is the railway vehicle operator's duty to decide on the maintenance actions to take [32].

Research has been performed in order to shift the focus of the regulations from the sizes of the defects to the magnitude of the impact loads that they generate. The influence of wheel–rail impact loads on the bending moment of rails has been evaluated in [36]. To determine whether a vehicle has to be removed from traffic for maintenance, it was concluded that a limit on measured wheel–rail contact force represents a better criterion than wheel flat length. In a subsequent study [37], the contact forces were related to crack growth in rails. The influences of variations in track stiffness, rail temperature and the presence of hanging sleepers were assessed. These studies contributed to the formulation of an updated recommendation for allowable dynamic wheel loads [38]. This particular specification specifies alarm limit depending on the difference between the current temperature of the rail and its stress-free temperature.

Updated regulations from Trafikverket are mainly based on peak impact loads registered at WILDs [39]. Impact loads exceeding the alarm levels are classified in three different categories depending on their magnitude. The load thresholds between these categories, however, are not fixed, but depend on whether the vehicle is a locomotive/power unit or a trailer coach/wagon. The thresholds can be lowered if the temperature is below -10 °C, if the ratio between the peak impact load and the static load is higher than some given limits or if the defect is longer than 90 mm [39].

2.4 Monitoring of track irregularities

Rails are also subjected to wear and fatigue damage, especially at the gauge corners and at locations where there is a significant tangential force between the wheel and the rail [40]. While rail wear affects the contact geometry, it can under some conditions have beneficial effects as initiated short cracks can be worn off before they start to propagate. This can be related to the existence of a "magic wear rate" [41],[42], i.e. a wear rate that is high enough to wear off surface cracks before they grow inside the material, while being low enough not to cause the system to not work any longer or to lead to component failure. Moreover, rail surfaces might be characterised by corrugation, i.e. a periodic irregularity along the longitudinal direction of the rail rolling surface. This will increase the dynamic wheel–rail loads.

Particularly critical rail locations from a fatigue perspective are welded sections, where residual tensile stresses from the welding process and potentially deteriorated geometry can be combined with the negative effects from voids, inclusions or other welding defects in the material [43]. Surface initiated rolling contact fatigue (RCF) can occur in the form of head check cracks on rails in curves. These cracks tend to propagate driven by traffic loading and the presence of fluid that gets trapped into the crack [44].

The formation of martensite at certain locations on the rail surface, or the presence of discrete defects, can trigger the formation of isolated forms of RCF damage on the rail surface. This is enhanced by the repeated application of traction and braking forces. The resulting defects are referred to as squats or studs [45]. Squats are characterised by the presence of a v-shaped crack and typically consist of an area where plastic deformation is combined with a network of subsurface cracks. Studs are squat-type defects that are generated by heat fluxes due to slip in the wheel–rail contact. Studs are not related to excessive plastic deformation, and while studs develop faster than squats, they are less likely to cause rail breaks [46].

Rails at rail joints and in switches & crossings (S&C) are often (more or less) affected by severe plastic deformation [47]. This may lead to an increase in vertical and lateral wheel–rail contact forces and the initiation of rail cracks..

The effective vertical and lateral positions of rail surfaces might differ from those of the original track design. This can be due to track settlement (deformation and degradation of the ballast and underlying soil), changes in rail profile (often due to wear or plasticity), and changes in geometry or position of other components of the track superstructure.

2.5 Monitoring of track characteristics

Infrastructure managers monitor the state of the track regularly. Track irregularities can be detected by special track monitoring vehicles (track geometry recording cars), which can use inertial and/or optical systems or mechanical transducers [15]. The rail profile at a specific section of the track can be measured using an extension of the MiniProf equipment [25] presented in Section 2.3.

In Sweden, the infrastructure manager (Trafikverket) post-processes the data obtained from track geometry measurements in order to obtain parameters that quantify track quality. One of these is the QS-ratio (Quality ratio for Standard deviation) [48]. This parameter is intended to provide a general assessment of the track quality for longer stretches, and it consists of a linear combination of the standard deviations of the differences in vertical and lateral positions of the rail from their nominal levels. This ratio has been used in **Paper D** as an indicator of track quality of the stretches where the instrumented wheelset had been travelling.

Track vertical stiffness (or flexibility) can be measured with track loading vehicles, which generate a static preload and a dynamic load on the track [15]. In other cases, only a dynamic load is generated (for example by means of an instrumented impact hammer). The track response varies depending on the preload, the frequency of the applied dynamic load as well as

the position within the sleeper bay where the track is being excited. The highest stiffness is measured for rail sections located above a sleeper, as discussed in **Paper A** and **Paper E**.

In **Paper D**, track stiffness measurements for the railway stretch connecting the Swedish towns of Partille and Alingsås are related to the high axle bending stress values detected by an instrumented wheelset. In this case, track stiffness was recorded based on an instrumented car which measured the vertical rail deflection over the studied section [49]. A smaller rail deflection is associated with a higher track stiffness.

3 Wheel–rail contact forces

The magnitudes of the forces generated in the wheel–rail contact should be limited as they can cause fatigue and damage to track and vehicle components. Excessive lateral track forces may also increase the risk of derailment. Contact forces can be separated into static forces (due to the axle load), quasi-static forces (for example those due to curving) and dynamic forces (mainly due to irregularities in track geometry, on the running surfaces of rails and wheel, in track stiffness, etc.) [50]. In this thesis, the focus is on the dynamic contribution to the wheel–rail contact forces.

3.1 Measurements

Wheel–rail contact forces can be measured in different ways. Since the 1960s, instrumented wheelsets have been used in Sweden to measure both vertical and lateral contact forces [51]. Instrumented wheelsets have been developed for different applications throughout the years [52] and are currently being used for condition monitoring of both the vehicle assets as well as of the track. In [53], for example, a track condition analyser (TCA) based on measured vertical and lateral wheel–rail contact forces was developed. This TCA is capable of recognising some types of track irregularities and rail surface defects by using a machine learning algorithm. Thus, the TCA can assess the track quality and the need for rail maintenance without disturbing the normal traffic operation.

Vertical contact forces can also be measured using wayside WILDs. These are capable of registering the mean and peak loads generated by the passage of each wheel. The data can be identified using the Radio Frequency Identification (RFID) tags of the vehicle and the date and time of the measurement and classified according to the direction of travel, the number of the axle in the vehicle and the speed of the train. By means of statistical analyses, WILD data can be used, e.g., to draw conclusions about the wheel tread deterioration rate in a specific axle [54]. In this thesis, WILD measurements have been used in **Paper E** to evaluate the effects of wheel tread damage on dynamic wheel–rail contact forces.

3.2 Simulations

Simulated contact forces can be used to provide relevant information on the status of trains and track. Several models and algorithms for the simulation of wheel–rail contact forces have been presented in the literature, see e.g. the overview in [55]. A general approach for solving the rolling contact problem, where discrete irregularities on wheels and rails are considered, is to use the finite element (FE) method in the time domain. However, such FE simulations carry high computational costs, in particular if a dense mesh of the wheel is employed and a long stretch of track needs to be considered. Computational times can be reduced substantially if the analysis is instead performed using a frequency-domain model. However, such models need to be completely linear. In studies where there is a large variation in contact force relative to the static wheel load, such as for the impact loads generated by the tread damage studied in the

present work, a non-linear contact model and calculations in the time domain are necessary [56].

In **Paper A**, **Paper B** and **Paper E**, the in-house MATLAB software WERAN (WhEel/RAil Noise) has been used for the simulations of dynamic wheel–rail interaction. More details on the software, as well as the theory behind the simulations, can be found in [11]. The algorithm and the equations behind the in-house software are also shortly summarised below.

In WERAN, the wheelset and the track are modelled by means of so-called Green's functions. This approach is also applied in tyre–road contact simulations, see [57]. In this thesis, the Green's functions for the wheelset and the track are obtained based on calculated frequency response functions using 3D FE models of the wheelset and the track.

For the wheelset model in Figure 13, the complex-valued (including information about both magnitude and phase) direct and cross receptances (displacement over force) are evaluated at both contact points to account for the dynamic cross-coupling (generated via the wheelset axle) between the two contact points. Once the receptance $R_{i,j}^{\mathrm{W}}(f)$ has been calculated at point i of the wheelset for a load applied at point j, the corresponding Green's function $G_{i,j}^{\mathrm{W}}(t)$ is calculated by means of an inverse Fourier transform symbolically expressed as:

$$G_{i,j}^{\mathrm{W}} = \mathcal{F}^{-1}(R_{i,j}^{\mathrm{W}}) \tag{1}$$

Since the rotation of the wheelset is not accounted for here, the Green's function $G_{i,i}^{\mathrm{W}}$ is equal to the impulse response of the radial displacement at point i due to radial excitation in the same position [58]. Neglecting the influence of wheelset rotation is a reasonable assumption according to [59]. Some examples of receptances and Green's functions for the wheelset in Figure 13 are plotted in Figure 14.

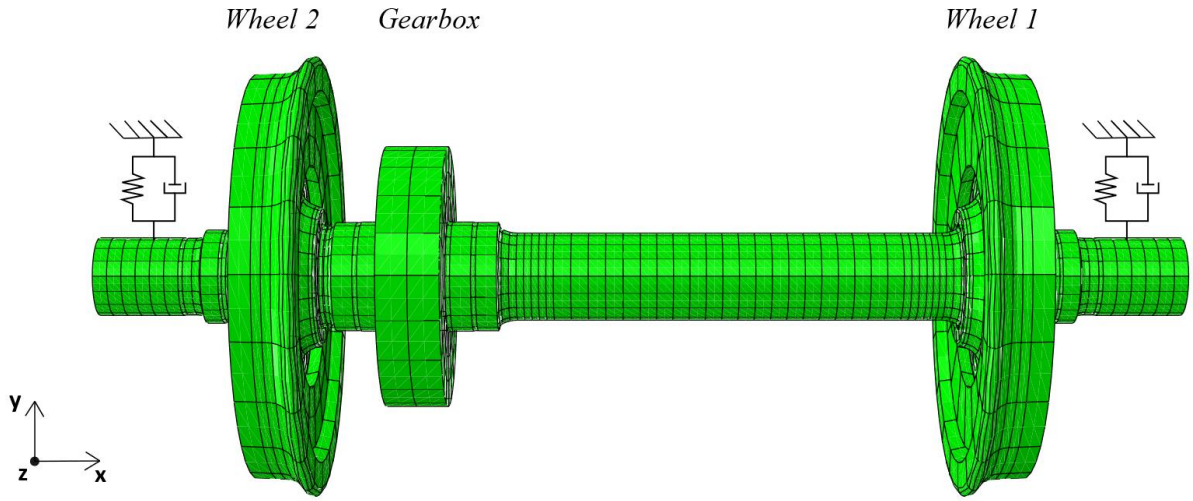

Figure 13: FE wheelset model used in **Papers A – D**. *Bearings and bearing boxes are modelled by point masses placed in the centre of the journals*

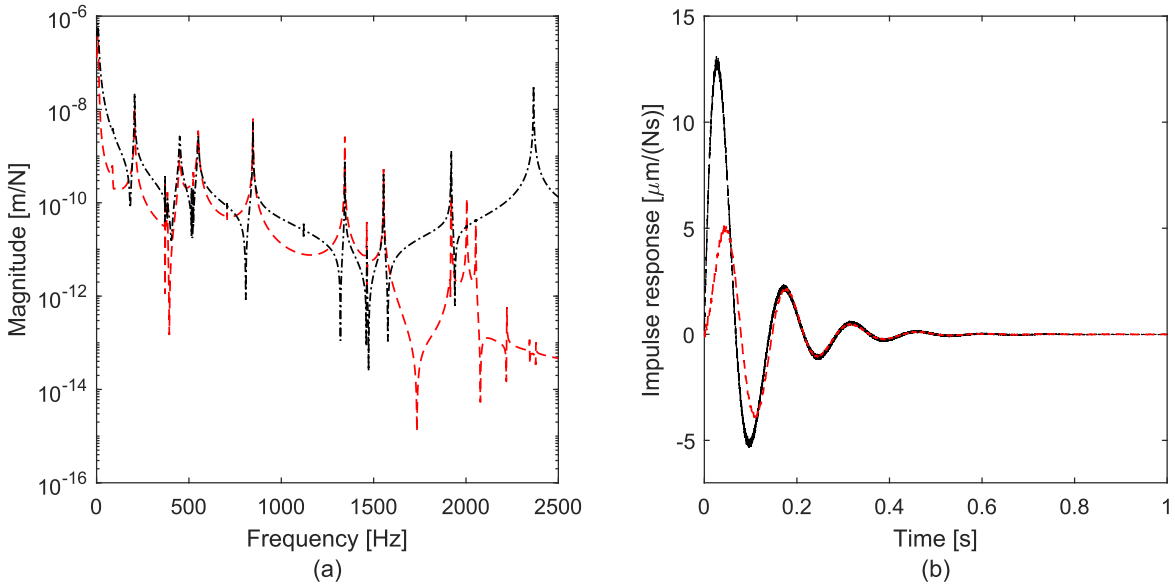

Figure 14: (a) Frequency response functions and (b) corresponding Green's functions for the wheelset model in **Paper A** *and* **Paper B**. *The direct receptance and its Green's function obtained for the wheel on the opposite side of the gearbox (named Wheel 1 in the papers) are plotted in black. The cross receptance in the contact point of the opposite wheel and its Green's function are plotted using a red dashed line*

A different mathematical formulation is necessary for the modelling of track dynamics to account for the relative longitudinal motion between the wheelset and the track. To make the equations more clear, the letters "W" and "R" are used in the symbols for receptances, Green's functions and displacements to clarify whether they have been computed for the wheelset or for the rail. In a first step, ordinary track Green's functions are computed from the direct and cross receptances at several track positions to capture the response of the track up to a sufficient distance from the contact point. For a set of receptances $R^{\mathrm{R},x_0,x_n}(f)$ computed at n sampling points x_n away from the loading position x_0, their respective Green's functions $G^{\mathrm{R},x_0,x_n}(t)$ can be computed as:

$$G^{\mathrm{R},x_0,x_n} = \mathcal{F}^{-1}(R^{\mathrm{R},x_0,x_n}) \tag{2}$$

These receptances also account for the dynamic cross-coupling between the two rails by the sleepers and the ballast and are obtained from a 3D track model whose cross-section is shown in Figure 15. For a given train speed v, samples from the set of ordinary Green's functions $G^{\mathrm{R},x_0,x_n}(t)$ are combined to form the discrete moving Green's functions $\tilde{G}_v^{\mathrm{R},x_0}(t)$ for the track [11],[60]. These account for the motion of the contact points along the rail. To construct discrete moving Green's functions for N_R number of samples, the relation between time increments Δt and space increments Δx ($\Delta x = v\Delta t$) is exploited as:

$$\tilde{G}_v^{\mathrm{R},x_0}(n) = \begin{cases} 0.5 \cdot \Delta t \cdot G^{\mathrm{R},x_0,x_0+[n-1]\Delta x}([n-1]\Delta t) & \text{for } n = 1, N_\mathrm{R} \\ \Delta t \cdot G^{\mathrm{R},x_0,x_0+[n-1]\Delta x}([n-1]\Delta t) & \text{for } n = 2, \dots, N_\mathrm{R}-1 \end{cases} \tag{3}$$

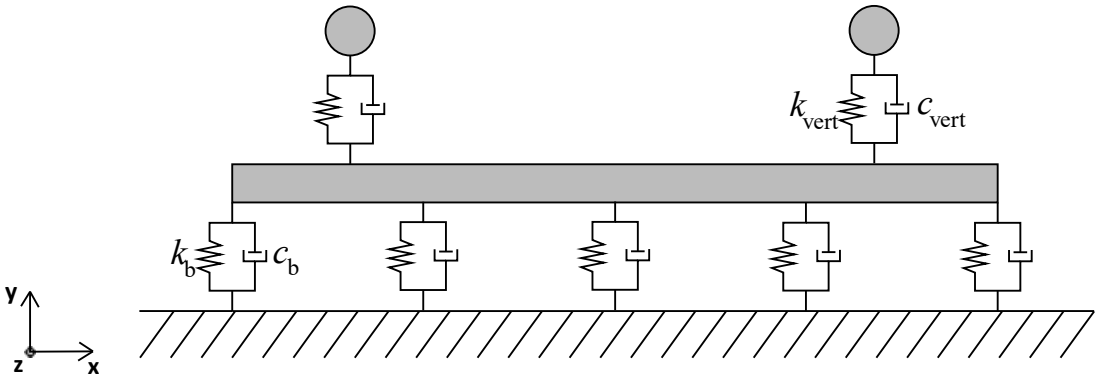

Figure 15: Cross-section of track model used in **Paper A**, **Paper B** *and* **Paper E**. *The view features one sleeper (the horizontal rectangle) and two rails (circles). The sleeper is connected to the ground by non-interacting springs and dampers coupled in parallel. Rail pads are modelled by accounting for both vertical and rotational (with respect to x, not shown in the figure) stiffness and damping*

Let $F_1(t)$ be the force acting in the contact point of wheel 1 and $F_2(t)$ the force acting in the contact point of wheel 2. The displacement $\xi_1^{\mathrm{W}}(t)$ of wheel 1 can then be computed as, see also Ref. [61]:

$$\xi_1^{\mathrm{W}}(t) = \int_0^t F_1(\tau) \cdot G_{1,1}^{\mathrm{W}}(t-\tau)\mathrm{d}\tau + \int_0^t F_2(\tau) \cdot G_{1,2}^{\mathrm{W}}(t-\tau)\mathrm{d}\tau \tag{4}$$

Similarly, for the displacement $\xi_2^{\mathrm{W}}(t)$ of wheel 2:

$$\xi_2^{\mathrm{W}}(t) = \int_0^t F_1(\tau) \cdot G_{2,1}^{\mathrm{W}}(t-\tau)\mathrm{d}\tau + \int_0^t F_2(\tau) \cdot G_{2,2}^{\mathrm{W}}(t-\tau)\mathrm{d}\tau \tag{5}$$

where $G_{1,2}^{\mathrm{W}} = G_{2,1}^{\mathrm{W}}$ due to reciprocity. A similar procedure is adopted for the displacements of the two rails $\xi_1^{\mathrm{R}}(t)$ and $\xi_2^{\mathrm{R}}(t)$, with the difference that here the moving rail Green's functions $\tilde{G}_v^{\mathrm{R},x_0}(t)$ are used [11].

The in-house software solves the normal contact problem using the active set algorithm proposed by Kalker [62]. At the interface between the two bodies, a potential contact area is defined and discretised into a mesh of *N* rectangular elements. In each time step, the elements that are in contact and their contact pressures are determined using an iterative procedure. The total vertical contact force $F_m(t)$ acting between wheel *m* and rail *m* (*m* = 1, 2) is computed by summing the contributions from the contact pressure values in all elements of the contact patch.

$$F_m = \sum_{I=1}^{N} p_{Iz}^m \cdot \Delta x \cdot \Delta y \tag{6}$$

The forces in the two contact patches are convoluted with their respective Green's functions to obtain the corresponding wheel ξ_m^{W} and rail ξ_m^{R} displacements, see Equations 4 and 5. It is assumed that the bodies in contact always have an elastic behaviour and that no plastification occurs. The iteration proceeds to the next step if the displacements are in agreement with the kinematic constraints for the wheel–rail contact, see Equation 7.

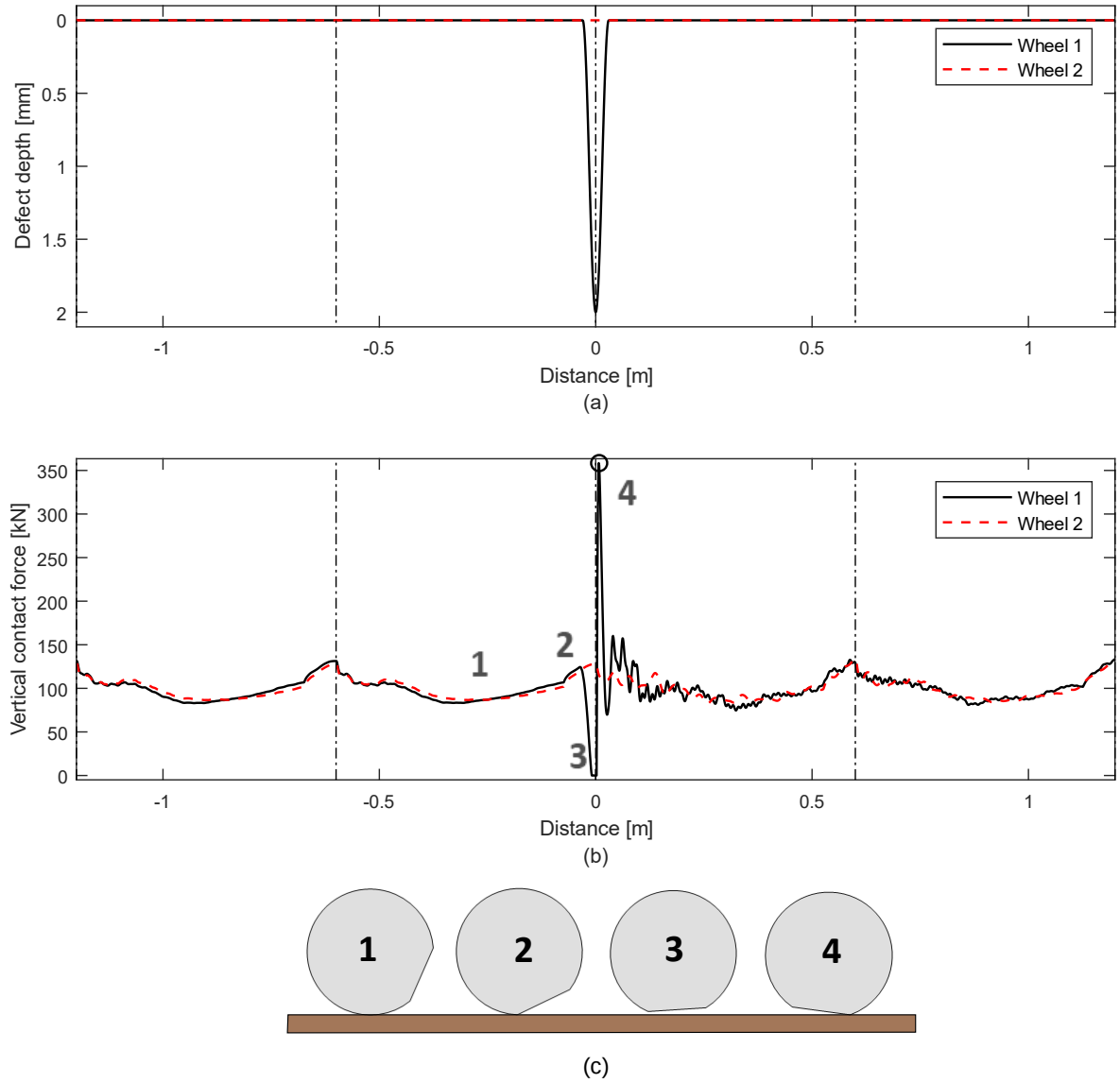

Figure 16: (a) Modelled irregularity at the nominal rolling circle of wheel 1, (b) calculated time history of vertical wheel–rail contact forces for both wheels, and (c) schematic representation of the relative position of the wheel tread defect with respect to the rail. Distance is measured from a point where the circumferential centre of the defect is aligned with a position on the rail directly above a sleeper. Axle load 20 tonnes and train speed 100 km/h. The vertical dashed-dotted lines indicate sleeper positions along the track. Maximum contact force is marked with a circle. Source: **Paper A**

$$d_{Iz}^{m} = \xi_{m}^{\mathrm{R}} + \xi_{m}^{\mathrm{W}} + u_{Iz}^{m} + z_{\mathrm{R},I}^{m} + z_{\mathrm{W},I}^{m} + r_{\mathrm{R},I}^{m} + r_{\mathrm{W},I}^{m} \tag{7}$$

Here d_{Iz}^{m} is the vertical distance between wheel *m* and rail *m*, $z_{\mathrm{R},I}^{m}$ and $z_{\mathrm{W},I}^{m}$ are the profiles of rail *m* and wheel *m*. For the *I*-th element of the potential contact area between wheel *m* and rail *m*, the total contribution in terms of deviations from the nominal geometry of wheel and rail due to roughness and discrete defects are denoted by $r_{\mathrm{W},I}^{m}$ and $r_{\mathrm{R},I}^{m}$. It is thus possible to account for the influence of discrete surface defects or other types of deviations from the nominal wheel/rail geometry, such as wheel and rail roughness or wheel out-of-roundness. Finally, u_{Iz}^{m}

is the displacement difference between the rail and the wheel. The cross-coupling between the two contact patches through the wheelset and the sleepers and ballast is accounted for in the Green's functions.

In the studies of **Paper A**, a discrete three-dimensional defect has been superposed on the tread of one wheel (labelled "Wheel 1" in Figure 13), see Figure 16(a). No defects were located on the opposite wheel or on the rail surfaces. The discrete defect had an ellipsoidal shape with maximum depth 2 mm, longitudinal semi-axis length 30 mm and lateral semi-axis length 24 mm. The defect was placed such that its longitudinal semi-axis was aligned with the wheel nominal rolling circle. For a speed of 100 km/h, Figure 16(b) shows the calculated time history of the wheel–rail contact forces for the two wheels. The time history of the damaged wheel resembles the oscillation in contact force due a wheel flat. As the wheel–rail contact reaches the leading edge of the tread defect, the wheel is subjected to an unloading phase, see Figure 16(c). For this combination of train speed and defect size, the contact force on the wheel with the tread defect is reduced to zero over a short time interval, implying that loss of contact has occurred. At the far end of the defect, the contact force for the damaged wheel increases abruptly to 358 kN. After the occurrence of the maximum force, a transient characterised by minor oscillations in magnitude is observed before the contact force returns to its original magnitude. Note that the wheel without the defect is only subjected to a minor variation in contact force, indicating that the cross-coupling between the contact points on the two wheels is rather weak.

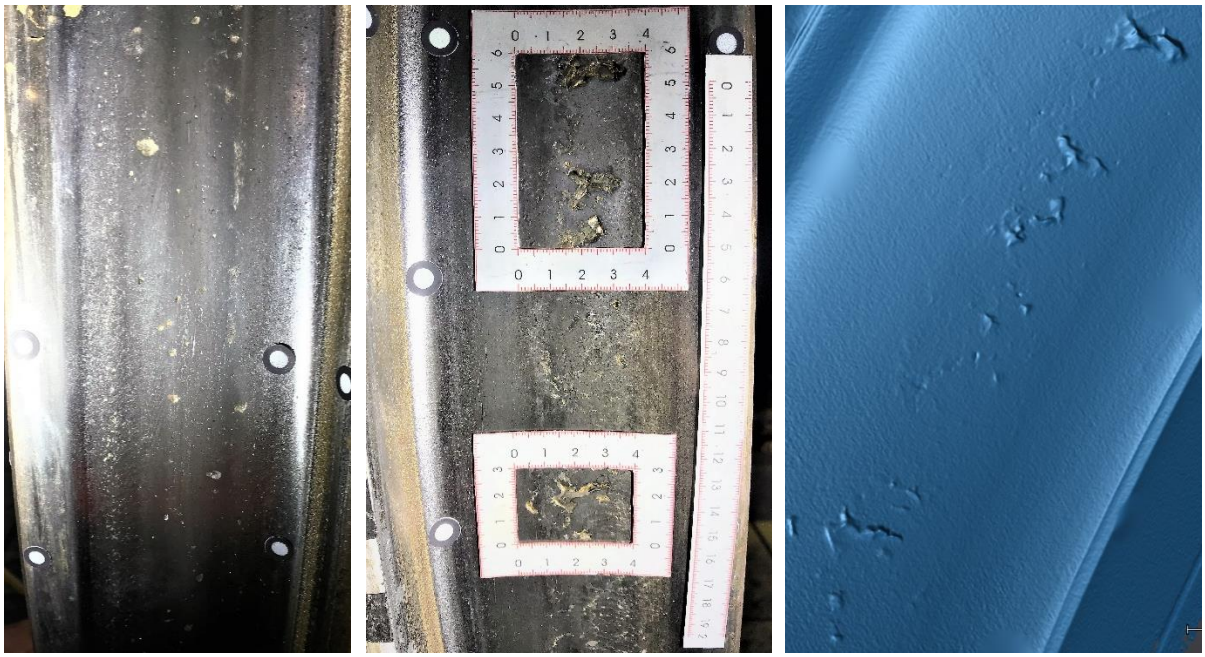

(a) *(b)* *(c)*

Figure 17: Wheel tread sections of the (a) less damaged wheel and (b) severely damaged wheel used in the field test and (c) surface geometry generated by scanning the severely damaged wheel. Source: Ref. [19] and **Paper E**

3.3 Influence of wheel tread damage

As discussed in the previous paragraph, damage on the wheel tread and/or on the rail running surface generates dynamic variations in the vertical wheel–rail contact force. Depending on the type of damage, the time history of the contact force can have a certain signature. For example,

as described in Section 3.2, a wheel flat initially generates a brief period of unloading of the rail, or even a temporary loss of wheel–rail contact for a large wheel flat. As the flat impacts on the rail, a sudden increase in contact load is generated followed by oscillations around the static value of the contact force [23].

Clusters of RCF defects may generate a more irregular signature of the vertical contact force depending on the distribution and shape of the discrete defects. According to the field test described in [19] and in **Paper E**, the peak force (maximum contact force over time) generated by a wheel with severe RCF seems to be proportional to the train speed up to velocities of 100 km/h, see Figure 17 [24]. The tread damage of the opposite wheel on the same wheelset was only characterised by some minor indentations, see Figure 17.

The field test was performed by Trafikverket and SJ in a collaboration to increase their understanding of wheel tread defects that trigger the alarm load limit in a WILD. The results from the field test, which are plotted in Figure 18, can be used to improve regulations regarding restricted operations, such as reduced train speed, after an alarm has been triggered.

The results from this field test have been used to verify the wheel–rail contact forces computed using the in-house software WERAN. Simulations were performed for the same operational conditions as those of the field test, as well as by accounting for possible variations in

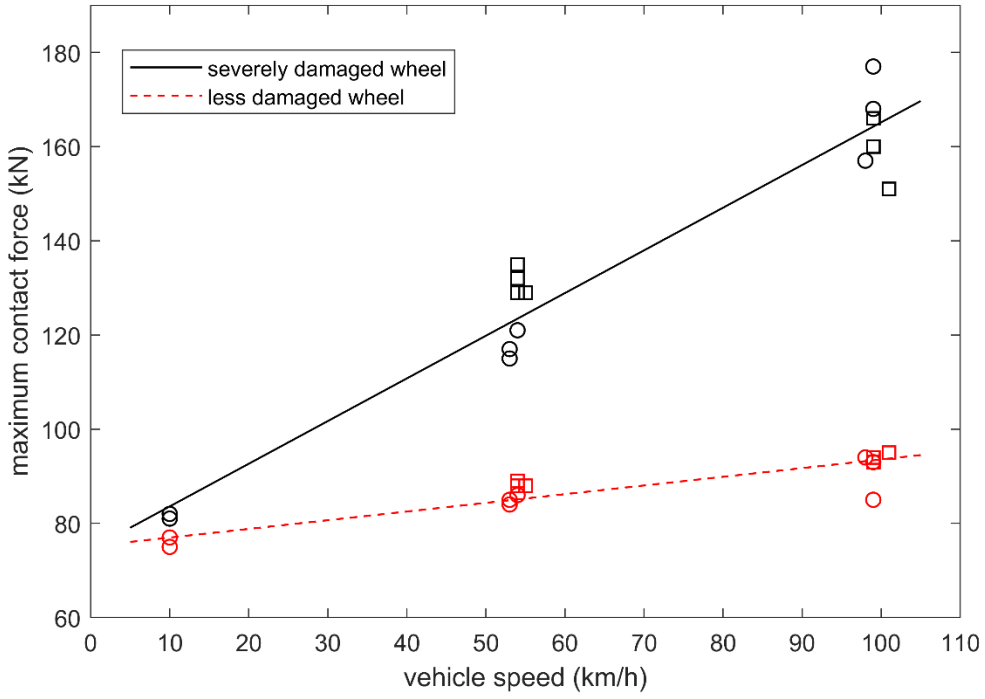

Figure 18: Peak loads measured during the field test described in **Paper E**. *The wheel which was severely affected by RCF damage is here referred to as "severely damaged wheel". The straight lines show the derived linear regression models*

parameters which were not controlled during the test (e.g. sleeper support stiffness, lateral contact position on the wheel, vehicle speeds above 100 km/h, etc.), see **Paper E**.

In Ref. [19], the largest RCF cluster present on the damaged wheel tread during the field test was modelled by superposing an ellipsoid-shaped discrete defect on the wheel tread according to the formulation in [63]. The defect had a maximum depth of 0.5 mm and semi-axis lengths of 60 mm in the longitudinal direction and 40 mm in the lateral direction. However, in **Paper E**, the influence of tread damage on wheel–rail contact forces could be assessed by accounting for the full 3D-scanned wheel tread in the contact model. In [19], the software only considered the contact conditions at one wheel–rail contact point.

In **Paper E**, time histories for some different forms of tread damage were analysed and compared. In a first study, the damaged wheel from the field test at Sunderbyn is investigated in more detail. It was observed that the tread damage could be described as a combination of local RCF damage clusters and a more longwave radial deviation from the nominal radius. In order to separately assess the effects generated by these two forms of discrete tread defects, the data obtained from the 3D scans has been post-processed to separate the long defect from the RCF clusters. To obtain the profile of the long defect, a low-pass filter was applied to the scanned mesh such that the more abrupt variations in geometry (those due to the RCF defects) were filtered out. The geometry of the RCF defects was obtained by taking the deviation between the scanned mesh and the low-pass filtered one.

The original scanned surface of the severely damaged wheel at Sunderbyn, see Figure 17(c), was employed in the simulation presented in Figure 19(a), while the results for the low-pass filtered surface and the RCF clusters are shown in Figures 19(b) and 19(c), respectively. In each figure, three wheel revolutions have been presented leading to a relatively periodic signature in which sleeper passages (every 60 cm) and RCF cluster position (every wheel revolution) can be identified. It is also clear that the time signature in Figure 19(a) can be seen as a combination of the lower frequency response due to the long defect and the higher frequency contributions due to the RCF damage, which also contains the general surface roughness that was present around the entire wheel circumference.

The reason why the deeper RCF defects studied here give a relatively low contribution to the impact load can be attributed to the contact filter effect, which becomes significant when the projected surface of the tread defect is smaller or on the same order as the size of the wheel–rail contact area. It can be concluded that, for the tread damage observed on the wheelset used in the field test at Sunderbyn, the long defect generates the dominating contribution to the high impact loads, whereas the influence of the various local RCF defects is minor.

Wheel OOR leads to oscillations in vertical wheel–rail contact forces and to the increase of rolling noise levels [64]. A particular type of periodic OOR is wheel polygonisation, which regularly has been found on wheels used in the Chinese high-speed rail network. Polygonisation can lead to a deterioration of the vehicle stability as well as to an increase of vibration levels in the bogie [65]. The lowest order types of periodic wheel OOR are eccentricity (which occurs when the wheel rotation axis is not coincident with the symmetry axis) and ovality. These types

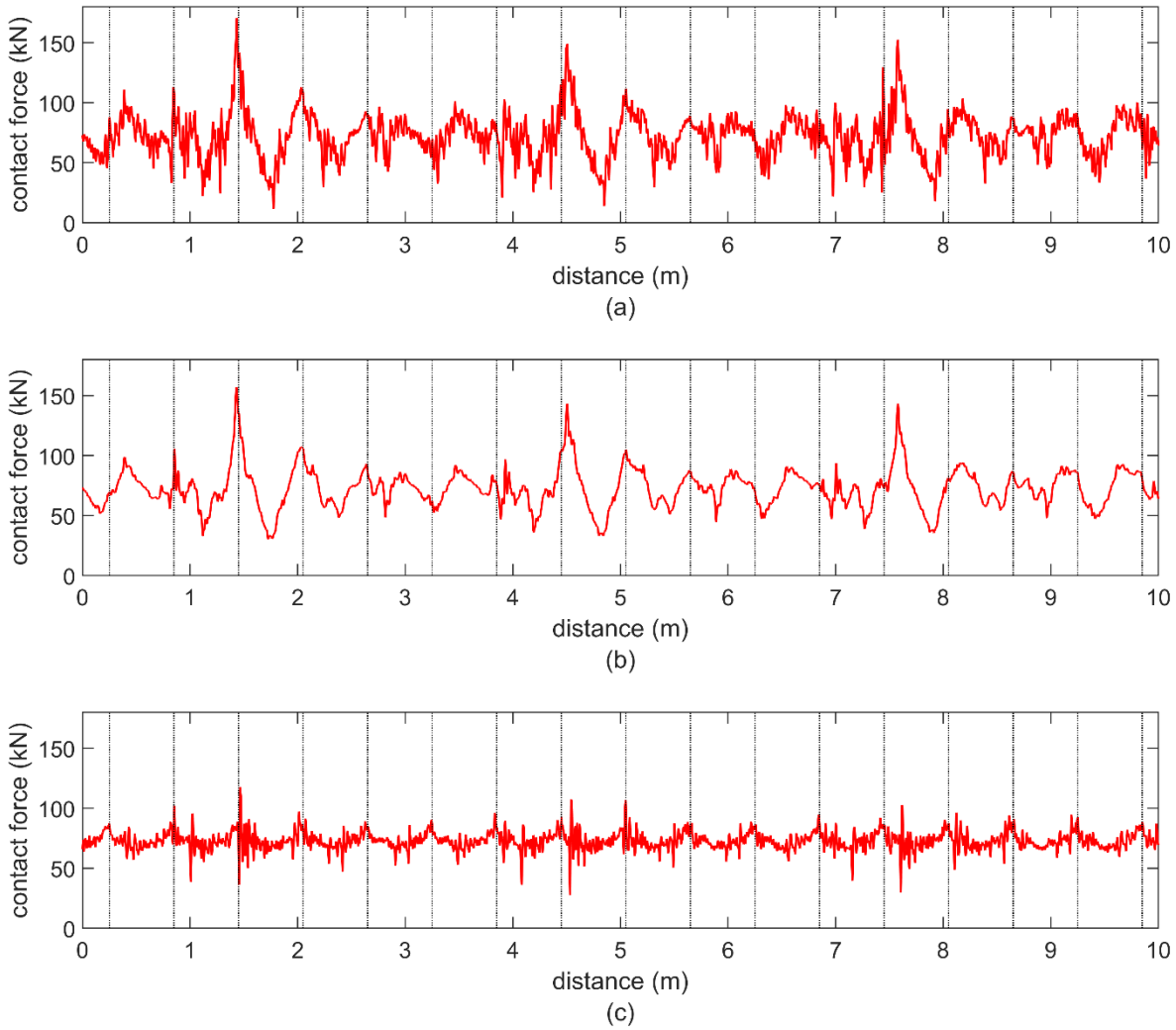

Figure 19: Calculated time histories of vertical wheel–rail contact force (in kN) for different surface geometries: (a) original scanned surface geometry of the damaged wheel from the field test at Sunderbyn, (b) low-pass filtered surface geometry of the same wheel, and (c) RCF defects on the same wheel. Train speed 100 km/h and rolling circle at wheel lateral coordinate -5 mm. Note that for (a,b), the trailing edge of the long defect, and (c) deepest RCF damage of the wheel tread damage were aligned with the sleeper located at 1.45 m from the start of the plot

of OOR were encountered (besides the already described RCF cluster) on the wheels used in the field test described in **Paper B**.

3.4 Influence of rail irregularities

The influence of rail roughness level on vehicle–track dynamics, and especially on the output in terms of rolling noise, has been investigated in several research projects, see e.g. [66] and [67]. The standard ISO 3095 [68] specifies the rail roughness level that is accepted in type testing of new vehicles in terms of their generated rolling noise levels. This is corresponding to a low-roughness rail that has been newly installed or recently ground (acoustical grinding). In

Paper B, rail roughness spectra inspired by the spectrum in ISO 3095 are employed to compute vertical wheel–rail contact forces generated by a given wheel out-of-roundness at different rail roughness levels. The results are also used to estimate the corresponding increase in axle stresses, as described in Chapter 4.

The effect of squats, as well as of discrete rail irregularities in general, on contact forces and local stresses have been investigated in depth in [63]. It was concluded that, while variations in contact pressure are mainly dependent on the three-dimensional shape of the defect, the tangential forces and shear stresses are highly affected by friction and creepages. It was also concluded that squats are more likely to be initiated by ellipsoid-shaped discrete defects rather than from corrugation on the rail.

S&C cause sharp variations in the wheel–rail contact geometry which can lead to significant impact loads. If the wheel is hollow-worn, these loads can be even higher [69]. High load magnitudes affect wheelset durability as well as the service life of the crossing. Indeed, accumulated plastic deformations, wear, RCF damage and track settlement in the S&C lead to a further magnification of wheel–rail contact forces [70].

Circular and transition curves generate different contact force signatures compared to S&C. Most curves do not lead to abrupt variations in the wheel–rail contact geometry and related high load magnitudes in contact forces. In fact, curves only tend to lead to a moderate increase of the dynamic contribution to vertical wheel–rail contact forces. However, elevated quasistatic lateral contact force magnitudes will occur. These forces are affected by the presence of cant deficiency or cant excess. Lateral contact forces generate additional stresses in the wheelset, which in the axle are superimposed on the bending stresses due to the vertical loading.

In **Paper D**, simulations have been performed using the multibody simulation software Simpack [71] for a Manchester benchmark passenger vehicle model [72]. For a given combination of vehicle speed and track superelevation, it is quantified how the vertical and lateral contact forces are redistributed between the inner and outer wheels with decreasing curve radius.

4 Stresses in the wheelset

Wheelset components are designed to sustain damage or fracture due to the high stresses emanating from the static and dynamic loads generated in the wheel–rail contact. As shown in the studies of **Papers A – E**, axles, wheels and bearings are subjected to high stresses due to the static weight of the vehicle as well as the lateral and vertical dynamic loads resulting from the dynamic wheel–rail interaction. In addition, torsional stresses due to braking or traction, and stresses generated by the shrink- or press-fit of the wheels on the axle and subsequent fretting contact between the axle and the wheel hub, contribute to the stress state.

4.1 Measurements

The evolution of stresses in the wheelset due to wheel tread deterioration can be investigated using field measurements. For example, measurements can be performed using instrumented wheelsets with strain gauges mounted on the axle or on the wheel web [52].

Research on instrumented wheelsets has been performed for wheelsets operating in the Chinese high-speed rail network. In [73], a system of strain gauges placed on both the axle and on the wheel web was developed with the objective to increase the signal-to-noise ratio and to obtain more precise measurements. In Italy, research has been carried out to increase the accuracy of measured wheel–rail contact forces for a wheelset running in critical conditions. A calibration procedure has been proposed to account for significant lateral displacements of the wheel–rail contact point. This can be appropriate for example when the derailment coefficient, i.e. the ratio of lateral force to vertical force acting on a wheel at a certain moment in time, is found to be high [74].

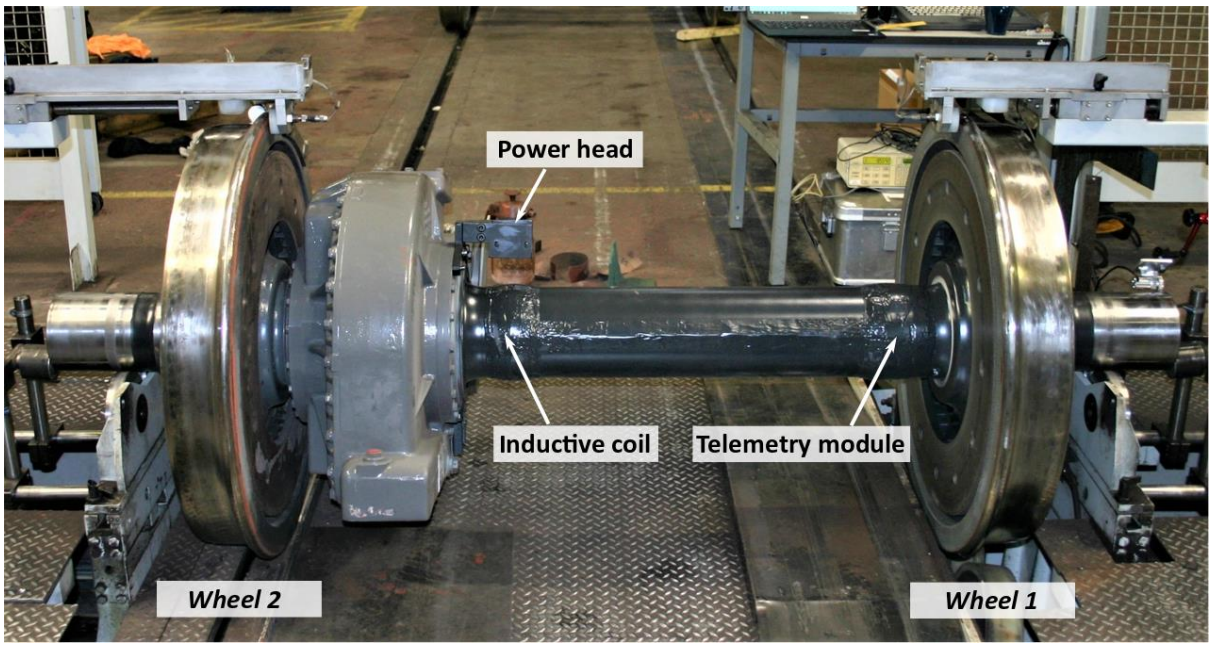

Figure 20: The instrumented powered wheelset used in the field test reported in **Papers B – D**. *Source:* **Paper B**

In **Paper B**, a system developed by Lucchini RS for the measurement of bending stresses at four different locations on the axle is employed. The system consists of strain gauges and a telemetry transmitter installed on the axle body, as well as a telemetry receiver, a telemetry inductive power supply and an embedded data acquisition computer installed in the bogie or on the vehicle body, see Figure 20. The strain data, which are processed on-board, are stored in the form of rainflow count data computed according to [75] for pre-defined combinations of intervals of mean values and amplitudes. The strains can be transformed to stresses by multiplication with a calibration coefficient. The rainflow data are uploaded to a remote server and can then be analysed using an axle crack-growth algorithm, such as the one presented in [76].

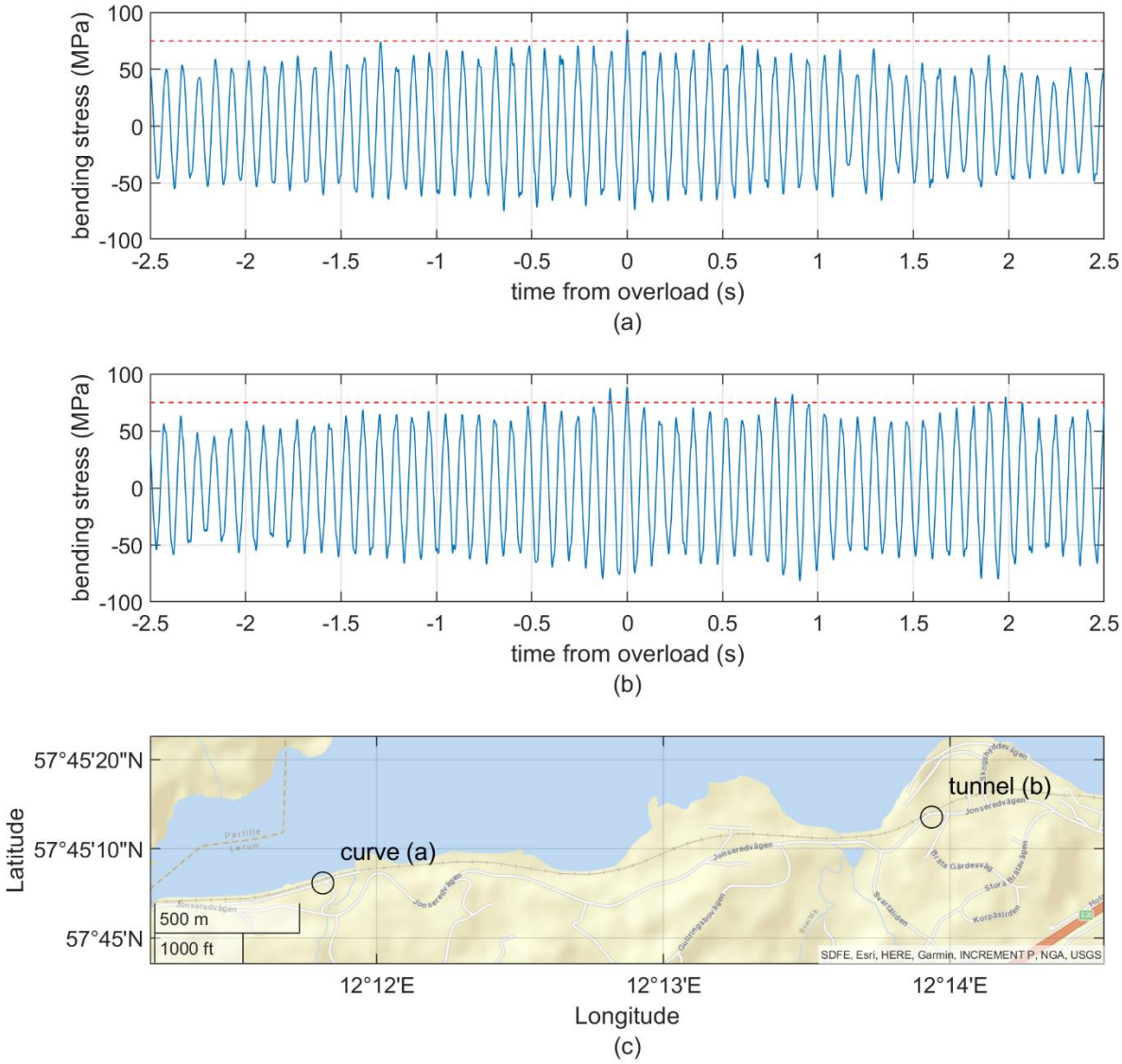

Figure 21: Measured time histories of axle bending stresses for a train ride over (a) a circular curve (R = 581 m) and (b) a transition curve (R = 585 m to R=583 m, but with opposite curvatures) in a tunnel. The horizontal red dashed lines indicate the stress threshold used in the study. The locations where peak loads have been registered for the two cases are marked in (c) in the map produced using MATLAB mapping toolbox [77]. Source: **Paper D**

The telemetry system algorithm has been recently updated and can identify bending strains that exceed a threshold level. These are named "overloads". Each time an overload is detected, five-second strain time histories centred at the instant of the overload are saved together with the date, time and GPS location of the detection. It is thus possible to study axle stress variations over time (see the examples in Figure 21), which can aid in understanding the cause of the overload.

The downloading of data pertaining to specific locations along the railway line allows to assess the influence of track (and wheel) quality on measured axle stresses for specific stretches of the track, see **Paper D**. Moreover, stress amplitude spectra collected at different times of the year can be used to investigate the effect of seasonal variations (such as variations in track stiffness between winter and summer) and/or the effect of performed maintenance (such as the influence of a decrease in running surface roughness after wheel reprofiling or rail grinding).

Different types of onboard condition monitoring sensors can be installed on passenger [12] and freight [78] vehicles. Accelerometers, for example, are relatively cheap and easy to install, but they cannot directly measure stresses. This thesis, instead, is mainly focused on stresses measured using a wheelset instrumented with strain gauges, such as the one in Figure 20. These measurements can be used to obtain service spectra for given track stretches, as is done in **Paper C**.

4.2 Simulations

To evaluate stresses in the wheelset, and in particular in the axle, different approaches for numerical simulations have been applied. In [79], axle stresses were computed by means of FE analyses based on the wheel–rail contact force magnitudes prescribed in [80]. A detailed FE model of a complete wheelset was used. Results in terms of stresses were post-processed using a crack propagation model based on Paris' law.

In [19], axle stresses were computed according to the quasi-static procedure described in the former standard for non-powered wheelsets [80]. For the studied axle, this procedure is the same as the one performed according to the current standard [81]. For different vehicle speeds, the average values of measured wheel–rail impact loads were used as input to calculate stresses at critical locations of the axle. If the contribution from the dynamic loads was neglected, it was concluded that the most critical section of the axle from a fatigue point of view was located at the fillet area near the brake disc. However, if accounting for the dynamic loads (but not the dynamics of the wheelset), other sections were subjected to higher stresses. At a speed of 100 km/h, the most critical sections were at the collar groove (the fillet located between the axle journal and the wheel seat) and at the wheel seat itself, where according to the standard the fatigue limit is reduced because of the effect of fretting.

In **Paper A**, based on calculated vertical contact force time histories (and the dynamics of the wheelset), a novel procedure for calculating time-variant stresses at critical locations of the wheelset is presented. In a first step, stress frequency response functions are computed using a 3D FE model of the wheelset, applying a similar procedure as the one used to obtain the

displacement frequency response functions briefly described in Section 3.2. Next, the stress frequency response functions (stress over applied force [Pa/N]) are transformed to stress Green's functions by means of inverse Fourier transforms. The complex-valued transfer functions, for each of the six stress components ($\sigma_{xx}, \sigma_{yy}, \sigma_{zz}, \sigma_{xy}, \sigma_{xz}, \sigma_{yz}$), can be computed at nodes of interest on the wheelset.

The stress frequency response functions $s_{ij}^{k,m}$ are computed at point *k* for the stress component σ_{ij} when the load is applied on wheel *m*. Then, each stress frequency response functions $s_{ij}^{k,m}$is transformed into a stress Green's function $S_{ij}^{k,m}$ by means of an inverse Fourier transform:

$$S_{ij}^{k,m} = \mathcal{F}^{-1}(s_{ij}^{k,m}) \tag{8}$$

The time history for a specific stress component σ_{ij} in the studied point *k* is determined by convolving the time histories of the contact forces $F_1(t)$ and $F_2(t)$ for the contact points on wheels 1 and 2 with the stress Green's functions $S_{ij}^{k,1}$ and $S_{ij}^{k,2}$:

$$\sigma_{ij}^{k}(t) = \int_0^t F_1(\tau) \cdot S_{ij}^{k,1}(t-\tau)\mathrm{d}\tau + \int_0^t F_2(\tau) \cdot S_{ij}^{k,2}(t-\tau)\mathrm{d}\tau \tag{9}$$

More details about the numerical implementation of this procedure are available in **Paper A**. Based on the time histories for the six stress components calculated at point *k*, e.g. the time history of the stress invariants in the studied nodes can be determined.

In **Paper B**, time histories of bending stresses in the axle have been computed, while (in a simplified way) accounting for the effect of the wheelset rotation. This was achieved by multiplying the time history of the stress amplitude with a time-variant cosine function having the same wavelength as the circumference of the rolling circle. These time histories have been

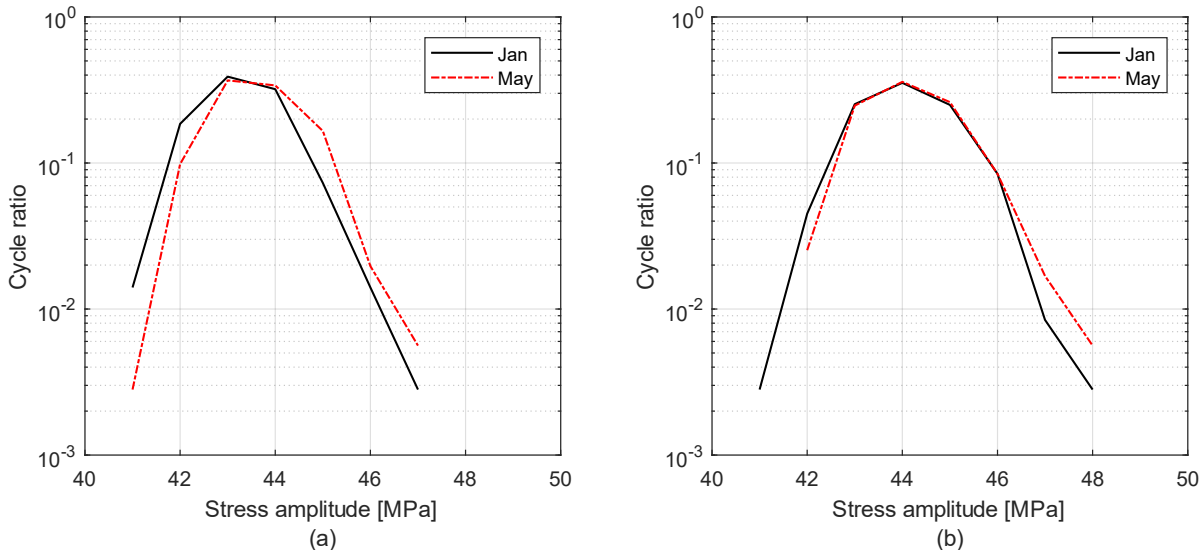

Figure 22: Simulated ratio between number of cycles at different stress amplitudes versus total number of cycles for OOR measured in January 2019 and May 2019 (a) 'Tangent track' and (b) 'Curved track' (R=500 m). Rail roughness based on ISO 3095 spectrum.
Source: **Paper B**

post-processed with a rainflow count algorithm to compute mean stresses and stress amplitudes at selected locations of the wheelset.

In **Paper B**, bending stress amplitudes have been computed at the location of the axle where the telemetry system was installed. Simulations were performed using the wheel OOR measured during the field tests performed in January 2019 and May 2019 as input for cases of running on tangent track and on curved track. The results are collected in histograms showing the occurrence of different stress amplitude values. Figure 22 compares stress amplitudes obtained from vertical wheel–rail contact forces computed for the different levels of wheel OOR (note that the peak-to-trough values of wheel OOR on the instrumented wheelset increased between January and May) and for the cases of running on tangent or curved track. More details on the simulation method are available in **Paper B**.

Figure 22 shows that an increase in the number of cycles at higher stress amplitudes can be observed for the cases representing 'Curved track' compared with the cases for 'Tangent track'. Note that the curving load case here implies the shifting of the vertical load towards a different rolling circle and not the application of a lateral load on the tread. Further, the simulations employing OOR from May 2019 lead to an increase in number of cycles at higher stress amplitudes compared with the simulations reflecting the OOR in January 2019. However, it is observed that the influence of wheel tread condition on the shift of stress amplitude spectra is relatively weak (in the order of 1 MPa). More studies have been performed in **Paper B** to distinguish between the increase in axle stresses due to the change in wheel OOR and the increase in stresses due to the lateral shift of the wheel–rail contact point on the wheel tread, e.g. due to curving or a change in the wheel tread conicity. It was concluded that the lateral shift had the larger influence on predicted stress magnitudes.

4.3 Stresses in axles

In Europe, axle design is regulated by the standard EN 13103-1 [81] (for axles with external journals). This standard has replaced the former standards EN 13103 [80] (for non-powered axles) and EN 13104 [82] (for powered axles). The calculations in this standard [81] are based on static design loads acting on the wheelset. Magnification factors are employed to account for the dynamic variation in loads (e.g. due to the effects of irregularities in track geometry and stiffness, braking, curving, traction, and S&C). The standard defines how fatigue stresses should be calculated at different sections of the axle (based on the axle geometry, information on vehicle dimensions, operating conditions, and braking or traction system) and how comparisons can be made with allowed stress levels for specific axle steel grades at specified axle zones. However, the employed design forces are independent of the actual train operating conditions, and dynamic variations in the wheel–rail contact forces due to tread damage and out-of-round wheels are not accounted for.

In this thesis, axle stresses have been studied referring to the guidelines from design standards [19], by using simulations based on the convolution integral approach (**Paper A** and **Paper B**), by using static or quasi-static FE analyses (**Paper D**), or by adopting a statistical approach

developed in the present project that is based on measured axle stress spectra (**Paper C** and **Paper D**).

During the field test performed with the instrumented wheelset in Figure 20, stress spectra have been collected for different stretches of "Västra Stambanan", a mixed traffic railway line connecting Gothenburg and Stockholm. These stress spectra plot the relative frequency of occurrence of given stress amplitudes. As the instrumented wheelset is installed under one end of a train that can travel in both directions, it will be subjected to different loadings depending on traffic direction. Higher loadings will be generated when the wheelset is travelling in the leading position. Thus, in order to account for the most detrimental loading, the studies in this thesis have mainly focused on stress spectra collected when the train was travelling in leading position.

In **Paper C**, axle bending stress spectra measured on different track sections have been used to estimate statistical distributions of axle stresses. Two truncated normal distributions, named P_1 and P_2, are fitted to the low stress and high stress parts of each measured stress spectrum, respectively (shown as the thick black line in Figure 23). The first part of the spectrum mainly consists of stress amplitudes between 35 MPa and 40 MPa, regardless of the travelling route. These stress amplitudes are mainly influenced by the (quasi-)static load acting on the axle. The last part of the spectrum is instead characterised by a rapid decrease of the occurrence of stress amplitudes. This decrease starts at different amplitude levels depending on the track section. In **Paper D**, these variations have been linked to differences in track properties.

The part of the stress spectrum located between the two truncated distributions has been modelled by a straight line in the semilogarithmic diagrams resulting in the distribution P_{mid}. The truncated distributions P_1, P_{mid} and P_2 form the full stress spectrum model, which is

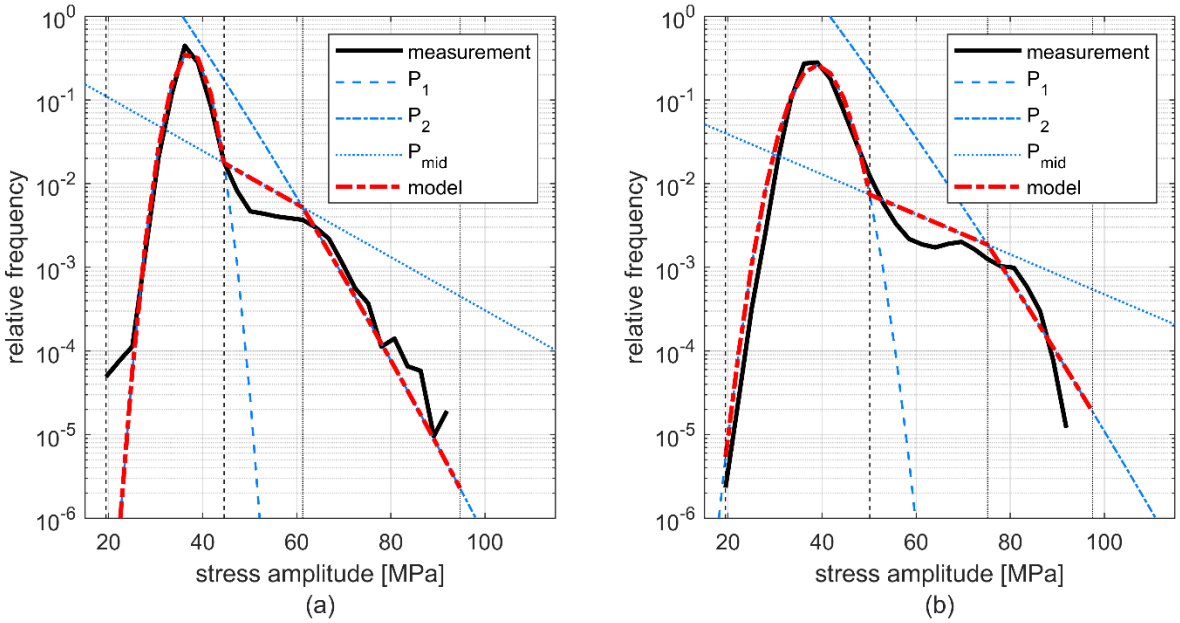

Figure 23: Relative frequency of occurrence of measured stress amplitudes, the probability distributions P_1, P_2 and P_{mid} and the resulting statistical model of the stress spectrum obtained for the railway lines (a) Hallsberg–Örebro and (b) Örebro–Västerås. A similar figure was produced in **Paper C** *for the lines Gothenburg–Skövde and Skövde–Hallsberg*

indicated by dashed red lines in Figure 23. In **Paper C**, these distributions have been used to generate stress time histories in order to assess the fatigue life of the wheelset. In **Paper D**, instead, the parameters describing the statistical distributions P_1 and P_2 have been correlated to track characteristics. Information on track properties (amount of S&C, lengths and radii of circular and transition curves, rail surface quality, presence of bridges and tunnels) was obtained for "Västra Stambanan" from the Swedish Transport Administration systems BIS [83] and Optram [84].

On given track stretches, a matching trend was found for the standard deviations of distributions P_1 and P_2 and the number of S&C per kilometre. S&C increase the dispersion of stress amplitudes in the measured spectrum and, in particular, generate high stress levels that shifts the "peak load distribution" P_2 towards higher stress amplitude values. Moreover, the number of registered overloads clearly increased for stretches with a higher presence of S&C.

A similar study was performed for circular and transition curves. It was noticed that regardless of whether the number or the total length of curves was used in the study, the results did not change significantly. Also, no significant differences were found between studying circular and transition curves separately or together. Curves with smaller radii, instead, tend to affect the standard deviation of stress distribution P_1 (the one in the vicinity of the axle static load) more significantly. It was concluded that curves do not generate very high contibutions to dynamic bending stress amplitudes as they do not lead to abrupt variations in vertical wheel–rail contact forces, see Paragraph 3.4. However, elevated lateral contact force magnitudes do occur during curving.

A correlation also seems to be present between the QS-ratio, see Section 2.5, and the standard deviations of the distributions P_1 and P_2. Moreover, the mean value and the standard deviation of distribution P_1 increase as the number of bridges and tunnels per kilometre increases. However, in these cases, the results might also be influenced by the presence of S&C, curves, etc. Some of the conclusions of the study are summarised in Table 1.

For a given railway line, the procedure that has been described here allows to predict a stress spectrum, which can later be adopted in the design of wheelset components as well as in maintenance planning. This is significant as service loads in real operations can be higher than those that can be determined according to the procedures suggested in the standards.

Table 1: Influence of studied track features on axle stress spectra. ++ indicates significant increase, + increase, and ○ that changes have no effect (i.e., a threshold level)

	switches & crossings	curves	track quality	tunnels and bridges
mean P_1	○	++	○	○
std dev P_1	+	+	+	++
mean P_2	○	○	○	○
std dev P_2	++	○	++	+

4.4 Stresses in wheels

Wheels are subjected to the combined effects from mechanical dynamic loads during service, centrifugal loads from wheel rotation and from residual stresses due to the heat treatment in the production, interference fit on the axle and subsequent operational loads. In [85], the growth of fatigue cracks in mono-block wheels was studied for different vertical loads, crack lengths and wheel–rail friction coefficients. As the initial length of a crack has a great influence on fatigue life, it was concluded that a more careful manufacturing process can increase the fatigue life of wheels remarkably.

During their production process, wheels are quenched by spraying liquid over their tread surface, but the hub, the disc and the rest of the rim are not quenched. The difference in cooling rate can generate a 100 – 130 MPa difference in tensile strength between the wheel rim and the wheel hub [86].

Stress variations in a wheel are analysed in detail in **Paper E**. Based on pre-computed vertical wheel–rail contact forces for different operational conditions and wheel tread damage distributions, the convolution integral approach is used to compute time-varying stresses in critical locations of the wheel web. Stresses due to lateral wheel–rail contact forces (e.g. during curving) are also considered in a simplified fashion.

In this work, three different locations on the wheel web have been studied, see Figure 24. Two of them are closer to the wheel hub and are respectively affected by tensile stresses (location A) and compressive stresses (location B) when the wheel is subjected to vertical loading at its nominal wheel–rail contact point. The third location (C) is close to the wheel rim and is mainly affected by compressive stresses. In order to account for the effect that the rotation of the wheel has on mean stresses over time, three extra locations located at the radially opposite positions on the wheel web were considered.

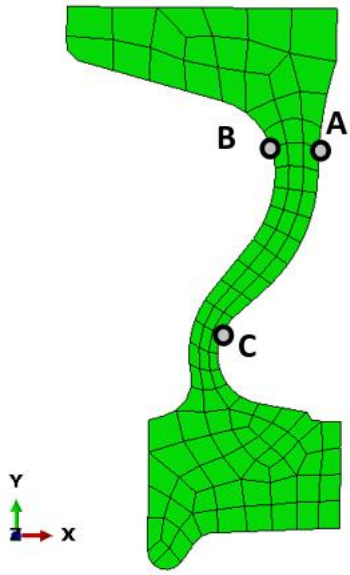

Figure 24: Cross-section of the wheel used in the field test at Sunderbyn with positions of locations where wheel stress time histories have been computed

Stress time histories for each location have been computed starting from the simulated vertical wheel–rail contact forces for the four studied tread damage cases. Then, in order to account for the rotation of the wheel, stress time histories for the radially opposite pairs of nodes at the three locations are alternated every half wheel revolution. After the time histories have been obtained for the six stress components, the Dang Van equivalent stress $\sigma_{\mathrm{eq,dv}}$ is computed as:

$$\sigma_{\mathrm{eq,dv}}(t) = \tau_{\mathrm{Tr,a}}(t) + \langle c_{\mathrm{dv}}\sigma_{\mathrm{h}}(t)\rangle \tag{10}$$

Here c_{dv} is a non-dimensional material constant ($c_{\mathrm{dv}} = 1/3$ in this work), σ_{h} is the hydrostatic stress and $\tau_{\mathrm{Tr,a}}$ is the Tresca shear stress computed from the "amplitude" (i.e. deviation from mid value during a stress cycle) of the deviatoric stress tensor, see Equation 11 where $\sigma^{\mathrm{d}}_{1,\mathrm{a}}$ and $\sigma^{\mathrm{d}}_{3,\mathrm{a}}$ are the maximum and minimum eigenvalues of the deviatoric stress "amplitude" tensor:

$$\tau_{\mathrm{Tr,a}}(t) = \frac{\sigma^{\mathrm{d}}_{1,\mathrm{a}}(t) - \sigma^{\mathrm{d}}_{3,\mathrm{a}}(t)}{2} \tag{11}$$

The term within Macaulay brackets $\langle c_{\mathrm{dv}}\sigma_{\mathrm{h}}(t)\rangle$ in Equation 10 is only accounted for when it has a positive value, i.e. in time instants when the hydrostatic stress is tensile.

As stress time histories have been calculated from vertical wheel–rail contact forces, the results relate to the case of a train travelling on a perfectly straight track. In Figure 25(a), it is possible to notice that Dang Van stresses increase at all the studied locations in the wheel disc for wheels with damaged wheel treads. However, in some cases the growth is more remarkable, for example for location "C" (see the yellow lines in Figure 25(a)). This can be expected as that

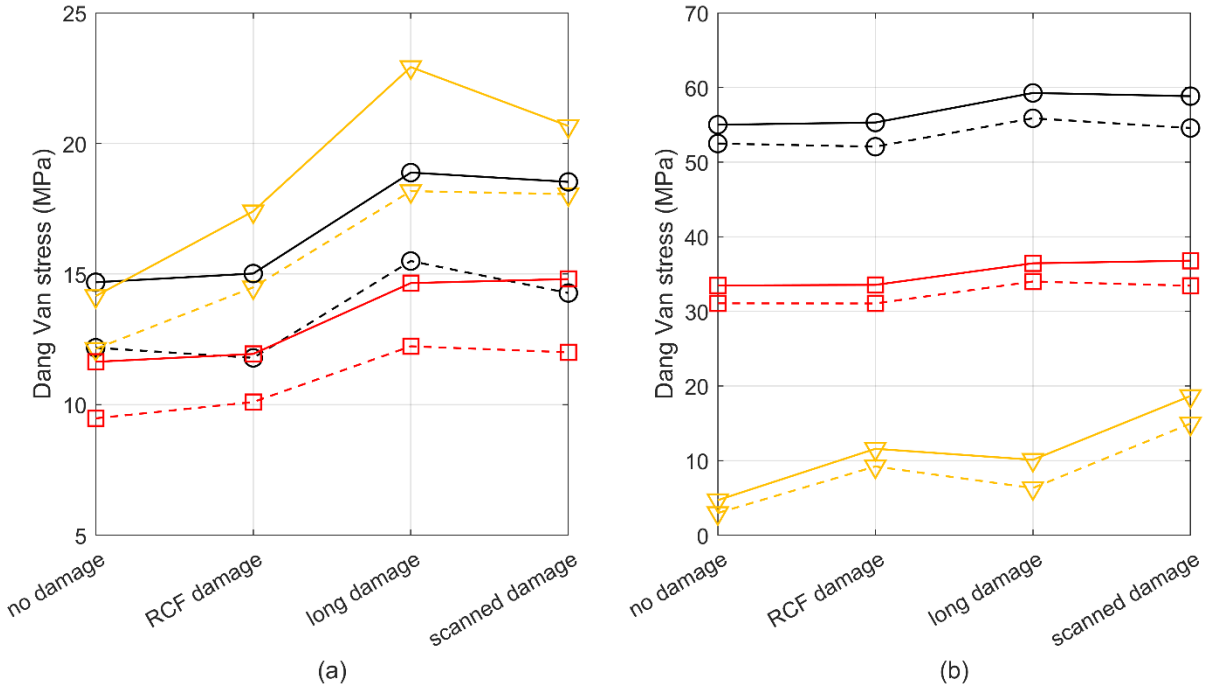

Figure 25: Median (dashed lines) and 90th percentile (solid lines) of Dang Van stresses computed for the wheel web locations "A" (black lines with circles), "B" (red lines with squares) and "C" (yellow lines with triangles) simulated for a wheel without damage and for the three types of damage studied in Figure 19. Vehicle running on (a) tangent track or (b) curved track

location is the closest to the wheel–rail contact point and the dynamic contributions from the contact forces have a larger influence there. Wheel locations where stresses are mainly compressive have lower Dang Van stress values because of the term within Macaulay brackets in Equation 10. Moreover, the frequency contents of the time-variant contact force lead to excitation of different vibration modes, which may generate higher stresses in some wheel locations.

To assess the impact of additional dynamic contributions to stresses during curving, some simulations have been performed where wheel stresses caused by vertical dynamic wheel–rail contact forces have been superposed to the static stresses generated by lateral loads due to curving. The magnitude and application point of these loads have been selected according to the guidelines in [87]. The results for the three studied locations are plotted in Figure 25(b). For locations "A" and "B", it can be observed that the increase in Dang Van stresses between the case with no damage and the case with the scanned damage is around 10%. However, this increase starts from a significantly higher value and can therefore be more significant for fatigue initiation.

The risk for subsurface initiation of RCF in the wheel rim is assessed in **Paper E** using the method developed in [88]. In that work, a simplified fatigue index FI_{simp}, which can be used in real time to predict initiation of subsurface RCF (and may be integrated with measurements from instrumented wheelsets), was developed starting from the general formulation of the subsurface RCF initiation index FI_{sub} presented in [89]. More details about the theory behind the index, as well as on how the parameters in the equation have been computed for the wheelset used in the field test at Sunderbyn, are available in [88] and in **Paper E**.

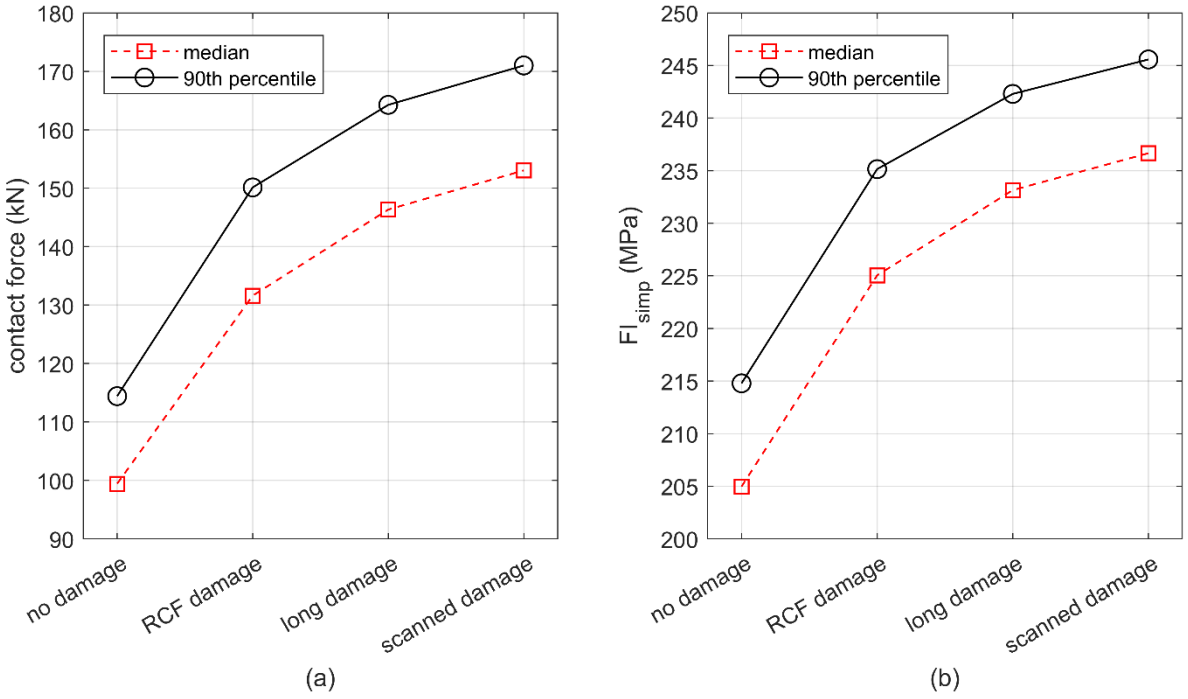

Figure 26: Median (dashed red line) and 90th percentile (solid black line) of (a) the vertical wheel–rail contact force and (b) the subsurface fatigue index FI_{simp} simulated for a wheel without damage and for the three types of damage studied in Figure 19.

The median values and the values corresponding to the 90th percentile of the calculated distributions of contact forces and FI_{simp} have been plotted in Figure 26 for the case of a wheel with nominal geometry as well as for the three damage cases studied in Figure 19. As expected, FI_{simp} increases with increasing level of contact force. However, due to the cubic root in Equation 2, an increase of around 50% in contact forces leads to an increase of about 15% in FI_{simp}. On the other hand, due to the exponential nature of fatigue damage laws, a relatively small increase in FI_{simp} can lead to a significant shortening of the fatigue life of the wheel rim.

4.5 Loads on bearings

In **Paper E**, the loading on the bearings has been computed based on pre-calculated wheel–rail contact forces. In this case, the loading is expressed in terms of the vertical forces acting on the axleboxes. Note that as a non-powered trailing wheelset was used during the field test at Sunderbyn, it was reasonable to assume that cylindrical roller bearings were mounted and that the effect of lateral forces could be neglected.

The vertical displacement of the axlebox located closest to the damaged wheel was computed by applying the convolution integral approach to the pre-calculated wheel–rail contact forces and the displacement frequency response functions for the reference point modelling the axlebox mass. After the vertical displacement y_{axlebox} of the axlebox has been computed, the total vertical force F_{axlebox} acting on the axlebox is derived as:

$$F_{\mathrm{axlebox}}(t) = k_{\mathrm{s}} \cdot y_{\mathrm{axlebox}}(t) + c_{\mathrm{d}} \cdot \frac{dy_{\mathrm{axlebox}}(t)}{dt} \tag{12}$$

where k_{s} and c_{d} are the stiffness and damping coefficients of the primary suspension. It was found that the relative increase in the 90th percentile of axlebox force was in the order of 7% between the case of a wheel with no damage and the wheel with the scanned damage from Sunderbyn.

The increase in axlebox force due to the four studied cases is moderate compared to the corresponding increase in wheel–rail contact force. However, as mentioned in the discussion for the other wheelset components, small relative increases in loading can lead to significant variations in the resulting fatigue life.

The results have been compared to the assumptions in the simplified calculation procedure contained in the SKF Railway Technical Handbook [90]. According to that procedure, a dynamic magnification factor of up to 1.17 should be applied (depending on the safety margin taken when choosing coefficients). More details about this calculation procedure are available in **Paper E**.

5 Towards optimised wheelset maintenance

Many of the studies presented in this thesis are aimed at gaining more knowledge regarding the evolution of stresses in the wheelset for different types of tread damage and load cases. Being able to predict the state of stress and the remaining life for different components would allow train operators to optimise maintenance routines and reduce overall costs while increasing the availability of their vehicle fleet. In this chapter, some common approaches used in maintenance planning will be described. These will be discussed from a stress monitoring point of view.

5.1 How can information about stresses be used to optimise maintenance?

Different approaches can be adopted for the maintenance of an asset. One of these is called reactive maintenance and consists of the strategy of not repairing a component before it fails or reaches the end of its life [91]. This approach is not favourable if the failure of the component can lead to high costs, such as in many cases in the railway industry. For example, an axle fracture can lead to a derailment. This would imply high additional costs for the train and track operators and, in the worst case, loss of lives.

Most maintenance plans are based on preventive policies or fault-driven action [92]. Preventive maintenance (also referred to as planned maintenance) is performed by taking assets off-service at specific intervals in order to avoid unexpected failures. While this maintenance strategy allows to save on costs and downtimes due to catastrophic failures, it often implies that some assets are replaced while they still have a residual lifespan.

Traditionally, inspections of railway wheelsets have been scheduled depending on the mileage covered by the vehicle. This means that locomotives and wagons are inspected in depots at regular intervals depending on the local regulations and/or the company expertise. Maintenance can also be planned according to the design of the component. If a “safe life” design approach is used, the fatigue strength of the component and the stresses it is subjected to in service are used to estimate its residual fatigue life. Maintenance intervals are derived by applying a safety factor to the residual fatigue life. A “defect tolerant” design, on the other hand, is based on the estimated growth rate of a defect and its critical size. In this case, the inspection intervals are planned by applying a safety factor to the residual life of the detected defect. This means that fatigue cracks may develop, but to prevent failures these have to be detected before they grow to a critical size [93].

Predictive maintenance foresees faults or failures in a deteriorating system in order to optimise maintenance efforts. Predictive maintenance is based on three main steps: data acquisition, data processing and maintenance decision-making [94]. Sensors are used to collect data about the conditions of the system. The right time to intervene is based on the evaluation of such data by means of statistics from the past or from simulations. This approach is based on technology which connects sensor data with a remote system of data control. The advantage of a predictive approach is that maintenance works become more proactive, and thus effective and efficient [94].

If a condition-based maintenance approach is adopted, the condition of an asset is monitored continuously and maintenance is scheduled when an indicator shows a decrease in performance or indicates a possible upcoming failure [95]. The axle stress data gathered by the instrumented

wheelset described in **Paper B** can be employed, in combination with more data from other monitoring systems, to adopt either a condition-based maintenance approach for the wheelset (in that case maintenance is performed when stresses reach a limit) or a predictive maintenance approach. In the latter case, maintenance would be scheduled based on the evolution of the stresses over time or based on numerical predictions of how the deterioration of the axle increases in subsequent operations. In the same paper, the possibility to recognise wheel tread deterioration from data collected by the instrumented wheelset is tested by means of simulations.

A more flexible planning of maintenance could reduce overall maintenance costs as well as increase the availability of the fleet. Some applications in the railway industry allow for the planning of maintenance intervals according to the observed conditions of the asset. For example, in [19], information on the status of a wheelset was acquired by measuring the loads generated by the passage of the vehicle over a WILD. In **Paper B**, information was gathered by monitoring bending stresses at a specified section of an axle. Data collected by the instrumented wheelset described in **Paper B** can be used in combination with residual life estimation software, such as the one presented in [96]. Maintenance can thus be postponed as long as the monitored parameters fall within the intervals determined by regulations or company practice.

Integrated simulations of the deterioration of a complex structure can be done by using data from sensors as inputs to a large physical model. This is part of the idea of a so-called digital twin, which consists of a comprehensive physical and functional description of the component, product or system. It includes information and algorithms required to mirror the life of its corresponding physical twin [97]. Based on pre-computed wheel–rail impact forces, the work in **Paper A** includes the development and application of an in-house software for the simulation of wheelset stresses. In the future, such work can be included in a digital twin model of a wheelset.

The stress spectra estimated from the statistical distributions in **Paper C** can be used in a digital twin model to account for the stresses that have been experienced in service and thus to predict wheelset durability, allowing the train operator to adopt a predictive maintenance approach. In **Paper C**, moreover, fatigue analyses have been performed for different fatigue damage accumulation algorithms and different axle surface conditions, which are meant to account for different maintenance conditions. An example can be seen in Figure 27.

The fatigue life calculation algorithms can also be applied to stress spectra estimated for different track characteristics according to the correlations found in **Paper D**. This may help in identifying threshold levels in axle surface conditions for different train routes at which precautions need to be taken to avoid failures. Based on the results derived under different operational conditions, the planned maintenance can be scheduled to an earlier or later occasion, and priority can be given to wheelsets where the estimated residual fatigue life is more critical. This would result in a more efficient use of resources for the train operator, as well as in more flexibility in the usage of the fleet.

In **Paper E**, the scanned tread damage from [19] is used as input to the in-house software presented in **Paper A** to investigate the influence of train speed on impact loads generated by a discrete form of tread damage that is not characterised by a smooth surface geometry and/or by

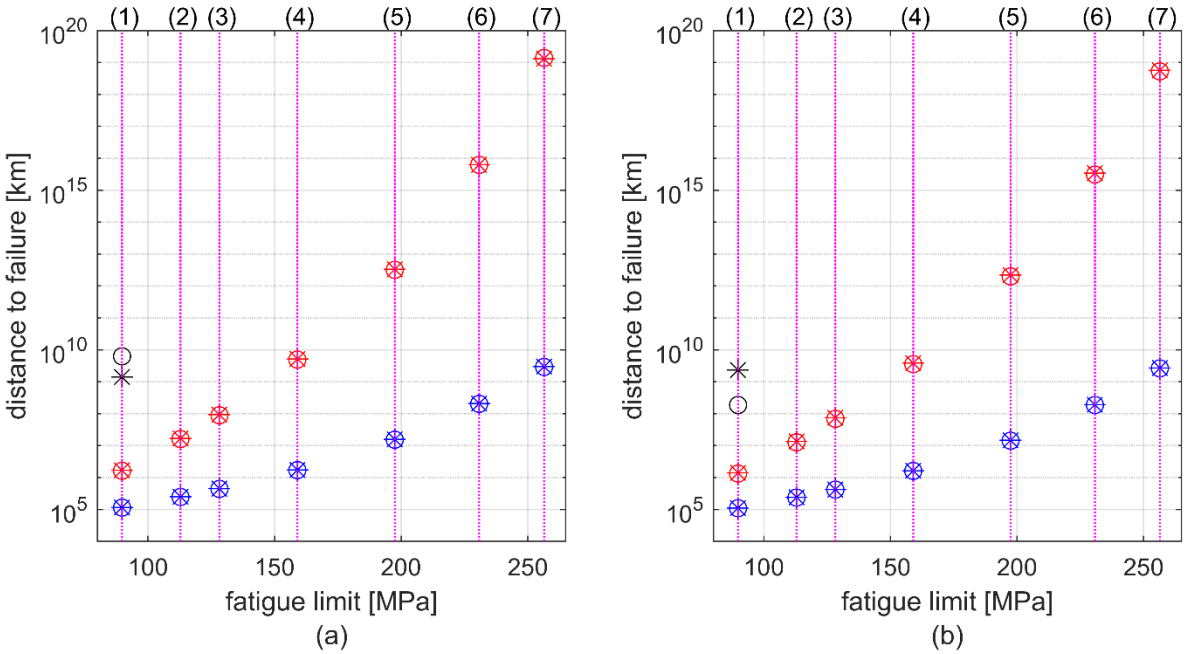

Figure 27: Estimated distance to failure for the instrumented axle for the stretches (a) Hallsberg–Örebro and (b) Örebro–Västerås. Fatigue lives marked with asterisks correspond to statistical models of stress spectra, while those marked with circles are obtained directly from field test spectra. Black markers indicate expected distances to failure if stress amplitudes below the fatigue limit are assumed not to cause any damage. Red and blue markers correspond to assumptions that there is no fatigue limit and the Wöhler curve continues after 10^7 cycles with one third of the original slope or with unchanged slope, respectively. Fatigue limits correspond to different axle surface conditions: (1) corroded in salt water, (2) as forged, (3) corroded in tap water, (4) hot-rolled, (5) machined, (6) fine-ground, (7) mirror polished. A similar figure was produced in **Paper C** *for the stretches Gothenburg–Skövde and Skövde–Hallsberg*

a uniform defect distribution over the wheel tread. The measured data are used for a verification of the simulation model and to achieve a better understanding of the influence of operational parameters on generated impact loads. The verified model can be used in a later stage to predict fatigue damage in the running gear caused by different wheel tread irregularities (wheel flats, RCF clusters and different types of out-of-roundness).

5.2 Future work

The implementations in the in-house software can be used to establish fatigue-stress spectra for running gear accounting for the influence of generic distributions and shapes of wheel tread irregularities. This should be useful for future wheelset design. The sensitivity to operational parameters can be investigated and critical parameters (such as types, sizes and shapes of tread damage as well as track characteristics such as presence of switches, track design, etc.) can be identified.

In particular, efforts should be put in characterising wheel tread damage and in coupling the geometry of the defect (e.g. depth, length) to operational parameters. This would for example be of help in applying a speed restriction for a train with a detected severe wheel tread damage. Operations could thus be carried out until maintenance is more convenient, without causing further damage to the track and running gear, and without jeopardizing safety.

Finally, more studies may focus on the relationship between data collected from sensors (regardless of whether they are installed on the vehicle or in the track) and the presence of wheel tread damage or track irregularities. The time histories of axle strain signals collected by instrumented wheelsets such as the one described in this thesis can be integrated in a calculation algorithm for damage accumulation in the wheelset. This would be of help for both the vehicle owner as well as the track manager while planning for maintenance, allowing to increase safety and punctuality while possibly optimising resources.

6 Summary of the appended papers

6.1 Paper A

An extension of the in-house software WERAN is presented, where both wheels in a wheelset and both rails in the track are included. The software is capable of accounting for generic distributions and shapes of wheel tread damage using a method that simulates the vertical dynamic interaction between wheelset and railway track at low computational cost. The influences of non-symmetric wheelset designs (such as the one for the powered wheelsets of an X40 train) and non-symmetric distributions of tread damage on the two wheels (or irregularities on the two rails) can be studied. Time-variant stresses are computed for the locations in the wheelset axle which are prone to fatigue. An extensive parameter study has been performed where wheel–rail impact loads and axle stresses have been computed for different distributions and sizes of tread damage as well as for different train speeds.

6.2 Paper B

A combination of instrumented wheelset measurements and numerical analyses of axle bending stresses is used to investigate the consequences of evolving RCF damage and wheel out-of-roundness on a passenger train wheelset. In a field test campaign, axle stresses have been monitored using a telemetry system with strain gauges installed on a powered wheelset mounted under an X40 passenger train. The evolution of wheel tread damage on that wheelset has been measured on regular occasions. The instrumented wheelset is described and some of the collected results in terms of stress amplitudes are presented. In a parallel study, the measured wheel out-of-roundness has been used as input to numerical simulations of vertical dynamic wheelset–track interaction and the evaluation of pertinent axle stresses using the approach developed in **Paper A**. Simulated and measured axle stresses are compared for cases involving different levels of rail roughness combined with the measured levels of RCF damage. The study enhances the understanding of how wheel tread damage and track quality influence axle stress magnitudes. In addition, the influence of the angular positions of the mounted strain gauges relative to the positions of the discrete wheel tread damage in terms of measured bending stresses is assessed through simulations.

6.3 Paper C

Axle bending strains measured using the instrumented telemetry system described in **Paper B** have been post-processed to obtain axle stress spectra for different track stretches. Statistical analyses are used to investigate the influence of changes in railway operational parameters on variations in the axle stress spectra. It is observed that stress cycles at higher amplitudes are affected by operational parameters such as track design, the number of S&C and whether the wheelset is in a leading or trailing position. The study indicates that a measured axle stress

spectrum can be replicated using truncated normal distributions. Spectra obtained directly from field tests, as well as spectra estimated from statistical distributions, are used as input to fatigue life analyses investigating damage accumulation in railway axles for different assumptions on the Wöhler curve. Results show good agreement between fatigue lives obtained from measured and statistically described stress spectra. It is concluded that fatigue damage can potentially initiate on axles suffering from corrosion or small surface cracks/scratches. The obtained statistical distributions of axle stresses can be used to predict the stresses that have been experienced in service. Fatigue analyses may help in identifying threshold levels in axle surface conditions at which precautions need to be taken to avoid failures.

6.4 Paper D

The stress spectra collected in **Paper B** and **Paper C** for different locations on the Swedish railway line "Västra stambanan", and the statistical distributions used to replicate them, are correlated to information on the corresponding track sections obtained from the Swedish Transport Administration databases. The same procedure is applied also for conditions generating peak stress levels. The study indicates that instrumented wheelset measurements can be used to compare the status of different track sections. It is concluded that S&C and other discontinuities in the track running surface lead to an increase in the number of overloads, while circular and transition curves lead to a shift of bending spectra towards higher stress amplitude values. The identified correlation between stresses measured in service and track characteristics can be used to predict stresses that (non-instrumented) wheelset would experience during service on stretches where the track characteristics are known. At the same time, variations in measured spectra can be used to identify and quantify track deterioration before more traditional measurements of track geometry etc. are performed.

6.5 Paper E

A field test in which a train was run at different speeds over a wheel impact load detector is described. One of the wheelsets in the train had severe wheel tread damage. The defects, including a combination of a large area on the wheel tread with a radial deviation from the nominal surface and also a cluster of RCF damage, have been scanned by means of 3D laser and their characteristics are described. The relation between the magnitudes of the impact loads measured for the damaged wheel and various operational parameters (speed and travelling direction of the vehicle, position in the sleeper bay where the defect strikes the rail, lateral position of the wheelset, track stiffness) is presented. The results are used to verify the in-house software for simulation of dynamic wheel–rail interaction. Based on simulated wheel–rail contact forces, wheelset stresses are computed for some forms of scanned tread damage and the effect on durability is assessed for the wheel discs, wheel rims and bearings.

7 Main results and conclusions

The aim of this thesis has been to enhance the understanding of the consequences of railway wheel tread damage and to identify better means of addressing them. To achieve this aim, numerical simulations of different operational scenarios have been crucial. The simulations of dynamic vehicle–track interaction were carried out in the time domain using a convolution integral approach based on pre-computed Green's functions, while the non-linear wheel–rail normal contact was solved using Kalker's variational method. In parallel, two extensive measurement campaigns with two different Swedish passenger trains have been carried out.

The main contributions of this thesis are:

- In **Paper A**, an existing numerical method to compute vertical wheel–rail contact forces has been enhanced by accounting for the dynamic cross-coupling (via the axle in the wheelset model and via the rail, sleepers and ballast in the track model) between the two contact points (one on each wheel). This means that non-symmetric wheelset designs and non-symmetric distributions of tread damage on the two wheels (or irregularities on the two rails) can be studied.

- In **Paper E**, the enhanced numerical method has been verified based on a field measurement campaign. Measured and calculated wheel–rail impact loads have been compared considering actual three-dimensional scans of the wheel tread damage.

- Based on pre-computed Green's functions, a routine for the post-processing of time histories of stresses at critical locations of the wheelset (including the dynamic stress contribution generated by wheel tread damage) has been developed in **Paper A**. In **Paper B**, calculated time histories of axle stresses have been compared to mean stresses and stress amplitudes measured by an instrumented wheelset. Good agreement between simulations and measurements has been observed.

- The numerical method has been applied to predict wheel–rail impact loads and stresses in the wheelset for generic distributions and three-dimensional shapes of wheel tread damage, see **Paper A** and **Paper E**. In **Paper E**, input to the model was based on a three-dimensional scan of the tread damage used in one of the measurement campaigns.

- For a given vehicle–track system, parametric studies have illustrated that the magnitude of the generated wheel–rail impact load depends on the three-dimensional shape of the tread damage, but also on other parameters such as speed and travelling direction of the vehicle, position in the sleeper bay where the defect strikes the rail, lateral position of the wheelset, and track stiffness, see **Paper A** and **Paper E**.

- For a given wheel tread damage, it was found that an increase in train speed leads to a substantial increase in wheel–rail impact load, while the influence on axle bending stresses is not as pronounced, see **Paper A** and **Paper B**.

- The studies in **Paper B** showed that variations in rail roughness level may lead to a significant influence on measured (and simulated) axle stresses, which may supersede the influence of the degradation of wheel OOR and generation of RCF clusters. This has implications on the condition monitoring of a wheelset.

- For the wheel tread damage measured on the instrumented wheelset, both the results from the simulation and the field test showed that, from a fatigue point of view, the variation in bending stress amplitudes was not significantly affected by the circumferential position of the sensors, see **Paper B**.

- A method to derive statistical descriptions of axle bending stress spectra using truncated normal distributions has been presented in **Paper C**. From these statistical distributions, simulated samples of bending stress histories can be obtained using a Monte Carlo approach.

- Spectra from the field test, as well as their statistical models, have been used as input to fatigue life analyses accounting for different assumptions for the Wöhler curve. Comparisons between fatigue lives obtained from measured and statistically described stress spectra showed good agreement. It was found that Monte Carlo-based fatigue life predictions converge after a relatively low number of stress samples generated from spectra, see **Paper C**.

- Results in terms of expected fatigue lives are heavily dependent on the hypotheses made on the reduction of the Wöhler curve for stress amplitudes below the fatigue limit. For example, the surface status of the asset has a large influence on the expected fatigue life, see **Paper C**.

- The method to derive statistical descriptions of stress spectra developed in **Paper C** has been employed in **Paper D** to characterise the loading on the instrumented axle while travelling over three different track stretches. The parameters describing the statistical model have been compared to some characteristics of the three stretches of track, for example track geometry deviations, amount of circular and transition curves, number of S&C, of bridges and tunnels, etc. This approach aids in identifying in a fast and cheap way what track characteristics that are related to changes in measured stress spectra. Thus, the developed simulation models can be used to predict stresses at critical locations of the wheelset and can be updated with measured data from onboard measuring devices, WILDs or other condition monitoring equipment.

- It was shown that statistical models of wheelset stress amplitude distributions provide an objective categorisation of the track section quality. For example, S&C were found to increase the occurrence of overloads generating higher stress amplitudes. Curves and transition curves increase the mean value of the stress amplitudes described by the distribution in the vicinity of the static axle bending load, but they do not generate abrupt variations in vertical wheel–rail contact forces, see **Paper D**.

- The methods and results obtained in **Papers A – E** can provide the train operator with a better understanding and a broader picture of the health status of their wheelsets. Results from connected simulations and measurements as well as real-time post-processing of data can be used to plan for more flexible maintenance intervals based on the observed condition of the wheelset.

References

[1] https://www.un.org/sustainabledevelopment/sustainable-development-goals/

[2] Johnson K L. The strength of surfaces in rolling contact. Proceedings of the Institution of Mechanical Engineers, Part C: Journal of Mechanical Engineering Science, vol 203, pp 151-163, 1989.

[3] Trafikanalys. Statistik 2022:35 Punktlighet på järnväg 2022 kvartal 3 (in Swedish: punctuality rate for railways during 3rd quarter of 2022). Trafikanalys, Stockholm, Sweden.

[4] Palmqvist C-W, Olsson N O E, Winslott Hiselius L. Some influencing factors for passenger train punctuality in Sweden, International Journal of Prognostics and Health Management, vol 8, 13 pp, 2017.

[5] Ekberg A, Paulsson B. INNOTRACK Concluding Technical Report. International Union of Railways (UIC), 288 pp, 2010.

[6] Pieraccini S. Strage di Viareggio, la ricostruzione di un disastro con 32 vittime. Newspaper article (in Italian: Viareggio, reconstruction of an accident with 32 fatalities), Il Sole 24 Ore, January 31st, 2017.

[7] Landucci G, Tugnoli A, Busini V, Derudi M, Rota R, Cozzani V. The Viareggio LPG accident: Lessons learnt, Journal of Loss Prevention in the Process Industries, vol 24(4), pp 466-476, 2011.

[8] D-RAIL Deliverable 1.1. Summary report and database of derailments incidents, http://d-rail-project.eu/, 71 pp + 3 pp appendix, 2012.

[9] Fraga-Lamas P, Fernández-Caramés T, Castedo L. Towards the Internet of smart trains: A review on industrial IoT-connected railways, Sensors, vol 17, 44 pp, 2017.

[10] Mehler U. Community response to railway noise: A review of social surveys, Journal of Sound and Vibration, vol 120, pp 321-332, 1998.

[11] Pieringer A. Time-domain modelling of high-frequency wheel/rail interaction, PhD thesis, Department of Civil and Environmental Engineering, Chalmers University of Technology, Gothenburg, Sweden, 107 pp, 2011.

[12] Li C, Luo S, Cole C, Spiryagin M. An overview: Modern techniques for railway vehicle on-board health monitoring systems, Vehicle System Dynamics, vol 55(7), pp. 1045-1070, 2017.

[13] Andersson E, Berg M, Stichel S. Vehicles. Book chapter, Rail Vehicle Dynamics, Railway Group KTH, Stockholm, Sweden, 28 pp, 2014.

[14] Andersson E, Berg M, Stichel S. Wheel-rail guidance mechanisms. Book chapter, Rail Vehicle Dynamics, Railway Group KTH, Stockholm, Sweden, 24 pp, 2014.

[15] Andersson E, Berg M, Stichel S. Track components, geometry and flexibility. Book chapter, Rail Vehicle Dynamics, Railway Group KTH, Stockholm, Sweden, 24 pp, 2014.

[16] Deuce R. Wheel tread damage – An elementary guide, Technical report 100115000, Bombardier Transportation GmbH, Germany, 38 pp, 2007.

[17] Ekberg A, Pålsson B. Multiscale modelling of train–track interaction phenomena with focus on contact mechanics, Wear, vol 430-431, pp 393-400, 2019.

[18] Nielsen J C O, Johansson A. Out-of-round railway wheels – A literature survey, Proceedings of the Institution of Mechanical Engineers, Part F: Journal of Rail and Rapid Transit, vol 217, pp 79-91, 2000.

[19] Maglio M, Asplund M, Nielsen J C O, Vernersson T, Kabo E, Ekberg A. Digitalisation of condition monitoring data as input for fatigue evaluation of wheelsets, Proceedings of the XIX International Wheelset Congress (IWC2019), Venice, Italy, 5 pp, 2019.

[20] Esmaeili A, Walia M S, Handa K, Ikeuchi K, Ekh M, Vernersson T, Ahlström J. A methodology to predict thermomechanical cracking of railway wheel treads – From experiments to numerical predictions, International Journal of Fatigue, vol 105, pp 71-85, 2017.

[21] Caprioli S, Vernersson T, Ekberg A. Thermal cracking of a railway wheel tread due to tread braking – Critical crack sizes and influence of repeated thermal cycles, Proceedings of the Institution of Mechanical Engineers, Part F: Journal of Rail and Rapid Transit, vol 227(1), pp 10-18, 2013.

[22] Jergéus J. Railway wheel flats – Martensite formation, residual stresses and crack propagation, PhD thesis, Department of Solid Mechanics, Chalmers University of Technology, Gothenburg, Sweden, 1998.

[23] Pieringer A, Kropp W, Nielsen J C O. The influence of contact modelling on simulated wheel/rail interaction due to wheel flats, Wear, vol 314(1-2), pp 273-281, 2014.

[24] Asplund M. Provkörning med hjulskada över hjulskadedetektor (in Swedish: Test run with wheel damage over a wheel damage detector), Technical report, Trafikverket, Luleå, Sweden, 18 pp, 2018.

[25] https://greenwood.dk/railway

[26] https://www.railmeasurement.com/tritops/

[27] https://www.creaform3d.com/en/portable-3d-scanner-handyscan-3d

[28] VX inspect and VX model, Creaform, Canada. https://www.creaform3d.com/en

[29] Gullers P, Andersson L, Lundén R. High-frequency vertical wheel–rail contact forces – Field measurements and influence of track irregularities, Wear, vol 265, pp 1472-1478, 2008.

[30] Jin X. A measurement and evaluation method for wheel-rail contact forces and axle stresses of high-speed train, Measurement, vol 149, 18 pp, 2020.

[31] Haji Abdulrazagh P, Hendry M, Roghani A, Toma E. Evaluating rail surface roughness from axle-box acceleration measurements: Computational metrology approach, Journal of Transport Engineering, Part A: Systems, vol 147(12), 13 pp, 2021.

[32] Larsson K. Wheel damage and maintenance of SCA Skog wagons. MSc Thesis, Department of Aeronautical and Vehicle Engineering, KTH, Stockholm, Sweden, 70 pp + 5 pp appendix, 2016.

[33] Byström R. BVF 592.11 Hantering av larm från stationära detektorer samt åtgärder efter upptäckta skador vid manuell avsyning (in Swedish: Management of alarms from stationary detectors and actions following damage detection during manual inspections), Trafikverket, Borlänge, 22 pp, 2015.

[34] Bruzell P. IBF 06:3 Trafiksäkerhetsinstruktion för Inlandsbanan AB (in Swedish: Traffic safety guidelines for the Inland track), Inlandsbanan AB, 4 pp, 2014.

[35] Samferdselsdepartementet. Forskrift om kjøretøy på det nasjonale jernbanenettet (kjøretøyforskriften) (in Norwegian: Indications for trains running on the national railway network), Samferdselsdepartementet, Norway, 2012.

[36] Kabo E, Ekberg A, Nielsen J C O. Analysis of static fractures of rails due to wheel flats, Research report 2009:01, Department of Applied Mechanics, Chalmers University of Technology, Gothenburg, Sweden, 22 pp, 2009.

[37] Kabo E, Ekberg A, Nielsen J C O. Alarm limits for wheel–rail impact loads – Part 2: Analysis of crack growth and fracture, Research report 2009:03, Department of Applied Mechanics, Chalmers University of Technology, Gothenburg, Sweden, 44 pp + 5 pp appendix, 2009.

[38] International Union of Railways (UIC). Prevention and mitigation of derailment (PMD), International Railway Solution 70729, 36 pp + 11 pp appendix, 2019.

[39] Asplund M. Larmnivåer Hjulskadedetektor TRV 2020/96962 (in Swedish: Alarm levels from wheel damage detectors), Trafikverket, Borlänge, 3 pp, 2021.

[40] Grassie S. Traction, curving and surface damage of rails, Part 2: Rail damage, Proceedings of the Institution of Mechanical Engineers, Part F: Journal of Rail and Rapid Transit, vol 229(3), pp 330-339, 2014.

[41] Vingsbo O, Söderberg D. On fretting maps, Wear, vol 126, pp 253-260, 1973.

[42] Kalousek J, Magel E. Achieving a balance: The "magic" wear rate, Railway Track Structures, vol 93(5), pp 50-52, 1997.

[43] Kabo E, Ekberg A, Maglio M. Rolling contact fatigue assessment of repair rail welds, Wear, vol 236-437, 8 pp, 2019.

[44] Ekberg A, Åkesson B, Kabo E. Wheel/rail rolling contact fatigue – Probe, predict, prevent, Wear, vol 314, pp 2-12, 2014.

[45] Grassie S. Studs and squats: The evolving story, Wear, vol 366-367, pp 194-199, 2016.

[46] Earl S, Rankin K E, Lewis R, Smith L, Rainforth W M. Comparison of squats and studs from different traffic environments, Proceedings of the 11th Conference on Contact Mechanics and Wear of Rail/Wheel Systems (CM2018), Delft, The Netherlands, pp 218-227, 2018.

[47] Ossberger U, Eck S, Stocker E. Performance of different materials in a frog of a turnout, Proceedings of the 11th International Heavy Haul Conference, Perth, Australia, pp 329-336, 2015.

[48] Optramförvaltningen. Datadokumentation och inställningsfiler i Optram (in Swedish: Data documentation and settings files in Optram), Trafikverket, Borlänge, 149 pp, 2022.

[49] Berggren E. Mätning av spårets nedböjning, Bandel 612, Alingsås–Partille (in Swedish: Measurement of the track deflection, Section 612, Alingsås–Partille), EBER Dynamics, Falun, 9 pp, 2021.

[50] Andersson E, Berg M, Stichel S. Track forces and derailment. Book chapter, Rail Vehicle Dynamics, Railway Group KTH, Stockholm, Sweden, 34 pp, 2014.

[51] Wrang M. Expanding the potential of load-measuring wheelsets, Railway Gazette International, Vol. 162, issue 9, 2006.

[52] Bracciali A, Cavaliere F, Macherelli M. Review of instrumented wheelset technology and applications, Proceedings of the Second International Conference on Railway Technology, Ajaccio, France, 16 pp, 2014.

[53] Gullers P, Dreik P, Nielsen J C O, Ekberg A, Andersson L. Track condition analyser: Identification of rail rolling surface defects, likely to generate fatigue damage in wheels, using instrumented wheelset measurements, Proceedings of the Instiution of Mechanical Engineers, Part F: Journal of Rail and Rapid Transit, vol 225(1), pp 1–13, 2011.

[54] Della Valle D. Railway wheel tread damage – Detection and consequences of wheel-rail impact loading, MSc Thesis, Department of Mechanics and Maritime Sciences, Chalmers University of Technology, Gothenburg, Sweden, 60 pp + 27 pp appendix, 2019.

[55] Knothe K, Grassie S L. Modelling of railway track and vehicle/track interaction at high frequencies, Vehicle System Dynamics, vol 22, pp 209-262, 1993.

[56] Nielsen J C O, Pieringer A, Thompson D J, Torstensson P. Wheel-rail impact loads, noise and vibration: A review of excitation mechanisms, prediction methods and mitigation measures, In: Geert Degrande et al. (editors), Noise and Vibration Mitigation for Rail Transportation Systems (*Proceedings of the 13th International Workshop on Railway Noise (IWRN13)*, Ghent, Belgium,

September 2019), Notes on Numerical Fluid Mechanics and Multidisciplinary Design, vol 150, 2021, pp 3–40.

[57] Andersson P. Modelling interfacial details in tyre/road contact – Adhesion forces and non-linear contact stiffness, PhD thesis, Department of Civil and Environmental Engineering, Chalmers University of Technology, Gothenburg, Sweden, 2005.

[58] Li X, Torstensson P, Nielsen J C O. Simulation of vertical dynamic vehicle–track interaction in a railway crossing using Green's functions, Journal of Sound and Vibration, vol 410, pp 318-329, 2017.

[59] Baeza L, Fayos Y, Roda A, Insa R. High frequency railway vehicle-track dynamics through flexible rotating wheelsets, Vehicle System Dynamics, vol 46, pp 647-659, 2008.

[60] Nordborg A. Wheel/rail noise generation due to nonlinear effects and parametric excitation, Journal of the Acoustical Society of America, vol 111, pp1772-1781, 2002.

[61] Li X, Nielsen J C O, Torstensson P. Simulation of wheel–rail impact loads and sleeper–ballast contact pressure in railway crossings using a Green's function approach, Journal of Sound and Vibration, vol 463, 16 pp, 2019.

[62] Kalker J. Three-dimensional elastic bodies in rolling contact. Kluwer Academic Publishers, Dordrecht, Boston, London, 238 pp, 1990.

[63] Andersson R, Torstensson P, Kabo E, Larsson F. The influence of rail surface irregularities on contact forces and local stresses, Vehicle System Dynamics, vol 53, pp 68-87, 2015.

[64] Johansson A. Out-of-round railway wheels – Assessment of wheel tread irregularities in train traffic, Journal of Sound and Vibration, vol 293, pp 795-806, 2006.

[65] Qu S, Wang J, Zhang D, Shi H, Wu P, Dai H. Field investigation on the higher-order polygon wear on wheel of high speed trains, Proceedings of the 11th International Conference on Contact Mechanics and Wear of Rail/Wheel Systems, Delft, The Netherlands, pp 818-823, 2018.

[66] HARMONOISE Deliverable 12, D12 Rail sources – Definition of track influence, 78 pp, 2005.

[67] Grassie S. Rail irregularities, corrugation and acoustic roughness: Characteristics, significance and effects of reprofiling, Proceedings of the Institution of Mechanical Engineers, Part F: Journal of Rail and Rapid Transit, vol 226, pp 542-557, 2012.

[68] ISO 3095:2013 Acoustics — Railway applications — Measurement of noise emitted by railbound vehicles. International Organization for Standardization, 2013.

[69] Milosevic M, Pålsson B, Nissen A, Nielsen J C O, Johansson H. Condition monitoring of railway crossing geometry via measured and simulated track responses, Sensors, vol 22(3), 26 pp, 2022.

[70] Liu X, Markine V, Wang H, Shevtsov I. Experimental tools for railway crossing condition monitoring (crossing condition monitoring tools), Measurement, vol 129, pp 424-435, 2018.

[71] Simulia, Simpack 2022 Documentation. Dassault Systemes, France, 2021

[72] Iwnicki S. Manchester benchmarks for rail vehicle simulation, Vehicle System Dynamics, vol 30(3-4), pp 295-313, 1998.

[73] Jin X. Evaluation and analysis approach of wheel–rail contact force measurements through a high-speed instrumented wheelset and related considerations, Vehicle System Dynamics, vol 58, pp 1189-1211, 2020.

[74] Cazzulani G, Di Gialleonardo E, Bionda S, Bassetti M, Crosio P, Braghin F. A new approach for the evaluation and the improvement of the metrological characteristics of an instrumented wheelset for the measure of wheel–rail contact forces, Proceedings of the Instititution of Mechanical Engineers, Part F: Journal of Rail and Rapid Transit, vol 231, pp 381-393, 2016.

[75] ASTM standard E1049 – 85. Standard practices for cycle counting in fatigue analysis, 10 pp, 2017.

[76] Beretta S, Carboni M, Cantini S, Ghidini A. Application of fatigue crack growth algorithms to railway axles and comparison of two steel grades, Proceedings of the Instititution of Mechanical Engineers, Part F: Journal of Rail and Rapid Transit, vol 218, pp 317-326, 2004.

[77] MathWorks Mapping Toolbox. https://it.mathworks.com/products/mapping.html

[78] Bernal E, Spiryagin M, Cole C. Onboard condition monitoring sensors, systems and techniques for freight railway vehicles: A review, IEEE Sensors Journal, vol 19(1), pp 4-24, 2019.

[79] Lundén R, Vernersson T, Ekberg A. Railway axle design – To be based on fatigue initiation or crack propagation?, Proceedings of the Institution of Mechanical Engineers, Part F: Journal of Rail and Rapid Transit, vol 224(5), pp 445-453, 2010.

[80] EN standard 13103:2001 Railway applications – Wheelsets and bogies – Non-powered axles – Design method. CEN – European committee for standardization, Belgium, 27 pp, 2001.

[81] EN standard 13103-1:2017 Railway applications – Wheelsets and bogies – Part 1: Design method for axles with external journals. CEN – European committee for standardization, Belgium, 52 pp, 2017.

[82] EN standard 13104:2009+A1:2010 Railway applications – Wheelsets and bogies – Powered axles – Design method. CEN – European committee for standardization, Belgium, 56 pp, 2010.

[83] Holmström P J. Användarhandledning BIS (Ban Informations System) (in Swedish: User guide for the track information system BIS), Trafikverket, Borlänge, 236 pp, 2019.

[84] Optramförvaltningen. Optram Användarmanual (in Swedish: Optram user manual), Trafikverket, Borlänge, 63 pp, 2021.

[85] Masoudi Nejad R, Farhangdoost K, Shariati M. Numerical study on fatigue crack growth in railway wheels under the influence of residual stresses, Engineering Failure Analysis, vol 52, pp 75-89, 2015.

[86] Poschmann I, Tschapowetz E, Rinnhofer H. Heat treatment process and facility for railway wheels, Zeitschrift für Werkstoffe, Wärmebehandlung, Fertigung, vol 62, 21 pp, 2007.

[87] EN standard EN 13979-1:2003+A2 Railway applications – Wheelsets and bogies – Monobloc wheels – Technical approval procedure – Part 1: Forged and rolled wheels. CEN – European committee for standardization, Belgium, 60 pp, 2011.

[88] Kabo E, Enblom R, Ekberg A. A simplified index for evaluating subsurface initiated rolling contact fatigue from field measurements, Wear, vol 271, pp 120-124, 2011.

[89] Ekberg A, Kabo E, Andersson H. An engineering model for prediction of rolling contact fatigue of railway wheels, Fatigue & Fracture of Engineering Materials and Structures, vol 25(10), pp 899-909, 2002.

[90] SKF Group. Bearing calculation, Book chapter, Railway Technical Handbook, Göteborg, vol 1,chapter 5, pp 106-121, 2011.

[91] Swanson L. Linking maintenance strategies to performance, International Journal of Production Economics, vol 70, pp 237-244, 2001.

[92] Cantini S, Cervello S, Gallo R. Traditional approach to wheelset maintenance. Book chapter, A modern approach to wheelset maintenance plan optimisation, Lucchini RS, pp 37-51, 2016.

[93] Zerbst U, Beretta S, Köhler G, Lawton A, Vormwald M, Beier H T, Klinger C, Černý I, Rudlin J, Heckel T, Klingbeil D. Safe life and damage tolerance aspects of railway axles – A review, Engineering Fracture Mechanics, vol 98, p 214-271, 2013.

[94] Selcuk S. Predictive maintenance, its implementation and latest trends, Proceedings of the Instititution of Mechanical Engineers, Part B: Journal of Engineering Manufacture, vol 231(9), pp 1670-1679, 2017.

[95] Ben-Daya M, Kumar U, Prabhakar Murthy D N. Condition-based maintenance, Book chapter, Introduction to maintenance engineering: Modeling, optimization and management, John Wiley & Sons Ltd, pp 355-387, 2016.

[96] Beretta S, Carboni M, Cantini S, Ghidini A. Application of fatigue crack growth algorithms to railway axles and comparison of two steel grades, Proceedings of the Instititution of Mechanical Engineers, Part F: Journal of Rail and Rapid Transit, vol 218, pp 317-326, 2004.

[97] Boschert S, Rosen R. Digital twin – The simulation aspect. Book chapter, Mechatronic futures, Springer, pp 59-74, 2016.